The tunable three section Distributed Bragg Reflector laser

Kennis, F.J.J.

Award date:
1996

7409

Eindhoven University of Technology

Department of Electrical Engineering
Telecommunications Division

THE TUNABLE THREE SECTION DISTRIBUTED BRAGG REFLECTOR LASER

master thesis of

F.J.J. Kennis

Philips Opto-electronics Centre
Eindhoven
September 1995 - June 1996

Advisor :
Dr. ir. A.A.M. Staring *Philips Opto-electronics Centre*
Supervisor :
Prof. ir. G.D. Khoe *Eindhoven University of Technology*

Preface

This report describes the work performed at Philips Optoelectronics Centre (POC), Eindhoven from September 1995 till June 1996, to obtain the Masters degree in Electronics Engineering from the Eindhoven University of Technology.

I want to express my thanks to my supervisor at the POC, dr.ir. A.A.M. Staring, for his advise and support. Furthermore, I want to thank prof. ir. G.D. Khoe and prof. dr. B.H. Verbeek for providing the possibility to carry out this work at the POC. Finally, I want to thank all other colleagues at Philips Research Laboratories and friends for making my time an enjoyable one.

Summary

Tunable 3 section DBR lasers are key components in coherent optical transmission systems and in Wavelength Division Multiplexing (WDM) systems. These lasers consist of a gain section and two tuning sections, respectively the PC- and the DBR section, and offer a wide tuning range while maintaining a high optical output power and a narrow linewidth, which is approximately independent of the emitted wavelength.

To examine the wavelength dependence of the output power, 3 parameters of the lasers have been varied: the composition of the active layer, the composition of the waveguide in the PC and DBR sections, and the pitch of the grating. To examine the differences in the properties of the lasers with these variations, the tuning-, power-, L-I-, and linewidth characteristics have been measured. With respect to a bulk active layer, it is shown that application of Quantum Wells in the active layer results in a higher output power, a lower threshold current and a narrower linewidth. Application of a waveguide layer in the PC and DBR sections with a bandgap that is close to that of the active section yields to some amplification in those sections, compensating for the losses due to the increase in free carrier absorption if the PC and DBR currents are increased. The optimum composition of this waveguide layer is expected to be found between $Q_{1.45}$ and $Q_{1.48}$ (near $Q_{1.48}$ for the bulk lasers, and near $Q_{1.45}$ for the quantum well lasers).

Modulation of any one of the 3 sections of the DBR laser by an a.c. signal results in an intensity variation in the output power (AM response) and a variation in the wavelength of the laser (FM response). The AM response of the gain section, as well as the FM responses of the PC and DBR sections have been investigated. It is shown that the AM and FM responses and their bandwidths are approximately the same for all devices. The FM responses and bandwidths of the PC and DBR sections are dependent on the pumping rate of these sections, and therefore vary with the output wavelength (high at low current, and low at high current).

The DBR laser can be used as a wavelength converter. If an input signal with wavelength λ_{in} is injected into the gain section of the laser, the signal is transformed as a result of cross-gain modulation to an output wavelength λ_{out}, which is tunable. An important parameter is the required input power for efficient wavelength conversion. Therefore, the output power as a function of the input power is measured for a number of devices. It is shown that the required input power for wavelength conversion can be reduced by applying a 10% coating on the gain section or by reducing the gain current. Furthermore, it is shown that extinction ratio enhancement can be obtained at low gain currents. Finally, some BER measurements have been performed to demonstrate wavelength conversion using a DBR laser.

Abbreviations and symbols

c	Speed of light	$[\mathrm{ms}^{-1}]$
c_1	Recombination constant	$[\mathrm{s}^{-1}]$
c_2	Recombination constant	$[\mathrm{m}^3\mathrm{s}^{-1}]$
c_3	Recombination constant	$[\mathrm{m}^6\mathrm{s}^{-1}]$
E_g	Bandgap	[eV]
f_bragg	Bragg freqency	[Hz]
f_m	Modulation frequency	[Hz]
f_Δ	FM deviation	[Hz]
g	Gain	$[\mathrm{m}^{-1}]$
g_th	Threshold gain	$[\mathrm{m}^{-1}]$
G_N	Gain derivative	$[\mathrm{m}^{-1}]$
h	Planck's constant	[Js]
$\hbar$	Planck's constant divided by 2π	[Js]
I_DBR	DBR current	[mA]
I_gain	Gain current	[mA]
I_m	Modulation current	[mA]
I_{PC}	PC current	[mA]
I_th	Threshold current	[mA]
$k_0,\ k_i$	Wavenumber	$[\mathrm{m}^{-1}]$
L_1	Length of the gain section	$[\mu\mathrm{m}]$
L_2	Length of the PC section	$[\mu\mathrm{m}]$
L_3	Length of the DBR section	$[\mu\mathrm{m}]$
L_cav	Length of the cavity	$[\mu\mathrm{m}]$
m	Longitudinal mode number	—
$n,\ n_1$	Refractive index	—
n_e	Effective-mode index	—
N_0	Carrier density at transparency	$[\mathrm{m}^{-3}]$
N_1	Carrier density gain section	$[\mathrm{m}^{-3}]$
N_2	Carrier density PC section	$[\mathrm{m}^{-3}]$
N_3	Carrier density DBR section	$[\mathrm{m}^{-3}]$
P_0	Output Power	[W]
r_1	Reflectivity facet gain section	—
r_4	Reflectivity facet DBR section	—
r_DBR	Reflectivity of the DBR section	—
R	Spontaneous recombination rate	$[\mathrm{s}^{-1}]$
$R_1,\ R_2$	Power reflectivity	—
S	Photon number	—
v_g	Group velocity	$[\mathrm{ms}^{-1}]$

α	Power absorption coefficient	[m^{-1}]
α_1	Power absorption coefficient gain section	[m^{-1}]
α_2	Power absorption coefficient PC section	[m^{-1}]
α_3	Power absorption coefficient DBR section	[m^{-1}]
α_{int}	Internal loss	[m^{-1}]
α_{m}	Mirror loss	[m^{-1}]
β	Complex propagation constant	[m^{-1}]
β_0	Bragg propagation constant	[m^{-1}]
β_{c}	Linewidth enhancement factor	—
$\lvert\Delta\lambda\rvert$	Separation of two longitudinal cavity modes	[nm]
η_i	Internal quantum efficiency	—
Γ	Confinement factor	—
κ	Coupling coefficient	[m^{-1}]
λ_m	Fabry Perot wavelength	[nm]
λ_{bragg}	Bragg wavelength	[nm]
λ_{in}	Input wavelength	[nm]
λ_{out}	Output wavelength	[nm]
Λ	Period grating	[nm]
ν	Frequency	[Hz]
Ω_{R}	Angular frequency of the relaxation oscillations	[rad s^{-1}]
Φ	Corrugation phase	[rad]
τ_{in}	Roundtrip time	[s]

AM	Amplitude Modulation
AOM	Acousto-Optical Modulator
AR	Anti Reflection
BER	Bit Error Rate
DBR	Distributed Bragg Reflector
DFB	Distributed FeedBack
EDFA	Erbium Doped Fiber Amplifier
FDM	Frequency Division Multiplexing
FM	Frequency Modulation
FP	Fabry Perot
FWHM	Full Width at Half Maximum
MZI	Mach-Zehnder Interferometer
PC	Phase Control
PRBS	Pseudo Random Bit Sequence
QW	Quantum Well
SIPBH	Semi Insulating Planar Burried Heterostructure
WDM	Wavelength Division Multiplexing

Contents

1. Introduction

Semiconductor lasers have played a major role as light sources in the rapid development of optical fiber communication systems. The almost unlimited bandwidth of the single-mode fiber provides great possibilities to build optical telecommunication networks with enormous bandwidths and high transmission speeds. Researchers are always trying to obtain longer transmission distances and higher transmission capacities. Often used technologies to this end, are coherent optical transmission and Wavelength Division Multiplexing (WDM). Key components in these technologies are tunable semiconductor lasers. The tunable laser can be used as a local oscillator in multichannel coherent Frequency Division Multiplexing (FDM) systems for the selection of a desired channel. They also find effective application in multichannel systems as transmitter sources and for optical switching in local area networks.

These tunable semiconductor lasers should offer a wide tuning range while maintaining a high optical output power and a narrow linewidth, preferably independent of the emitted wavelength. A three-section Distributed Bragg Reflector (DBR) laser is an example of such a device. It consists of a gain section and two tuning sections, respectively the phase- and Bragg section. These lasers offer a wide continuous tuning range (approximately 6 nm), and a large, wavelength independent output power (about 8mW in a single mode fiber).

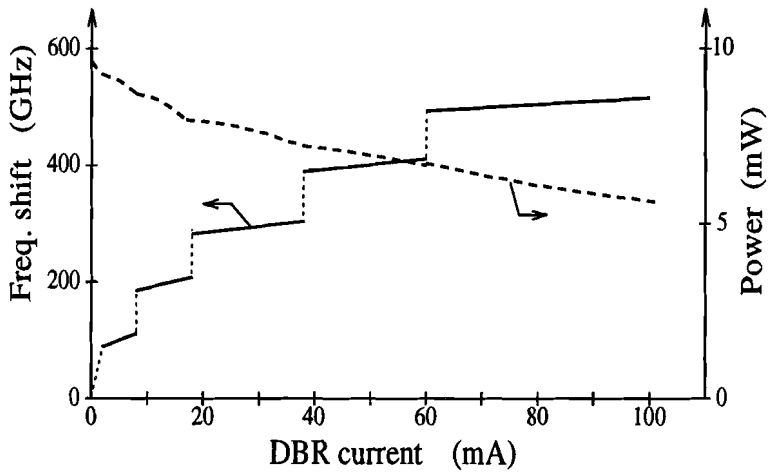

Figure 1.1: Frequency shift and output power versus DBR tuning current of one of the first 3-section DBR lasers. (After Ref. [1])

The early three-section DBR lasers suffered from a decrease in output power with increasing tuning current. As an example, in Fig. 1.1 the output power and frequency shift are given versus the DBR tuning current [1]. For this particular laser the power decreases from

10 mW to 6 mW. In more recently developed DBR lasers this effect is less pronounced [2]. One of the aims of the work presented in this report is to examine the conditions under which the power becomes as constant as possible over the entire tuning range.

An additional aim of the project is to examine the use of a tunable 3-section DBR laser as a wavelength converter. Optical wavelength converters transform an optical signal from one wavelength to another, and can be of use in optical WDM communication networks and optical switching. With the 3-section DBR laser it is possible to transform the signal to an output wavelength which is tunable over the tuning range.

After this introduction, in Chapter 2 the operation of a semiconductor laser is briefly explained, and the theory of the tunable 3-section DBR laser is outlined. In the Chapters 3 and 4 a describtion is given of the measurements of the static and dynamic properties of the 3-section DBR laser, including a comparison with the theory of Chapter 2. Chapter 5 covers the application of the 3-section DBR laser as a tunable wavelength converter. Finally, Chapter 6 gives some conclusions.

2. Theory of the tunable 3-section DBR laser.

2.1 Operation of a semiconductor laser.

A schematic diagram of a semiconductor laser is shown in Fig. 2.1. Between the p-type and n-type materials of the laser diode there is an active layer. When a current flows through the laser, electrons and holes are injected into the active layer, where they recombine through radiative and non-radiative mechanisms. Photons of energy $h\nu \cong E_g$ are emitted as a result of radiative recombination. However, these photons can also be absorbed through a reverse proces that generates electron-hole pairs. When the current exceeds a critical value the rate of photon emission can exceed that of absorption. This condition is called population inversion. If a photon enters the inversion region, it can stimulate the emission of another photon having the same phase and frequency. The total optical power in the active region is increased by this stimulated emission mechanism and the active region is said to exhibit optical gain.

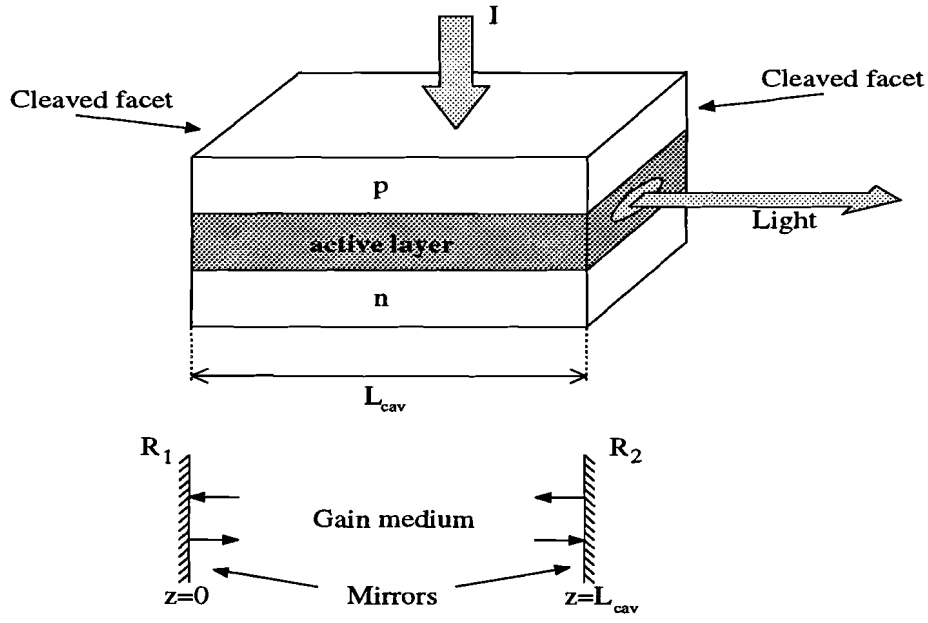

Figure 2.1: **Schematic diagram of a semiconductor laser and Fabry-Perot (FP) cavity. The cleaved facets act as partially transparent mirrors.**

Optical gain by itself is not enough to make a laser lase. In addition, an optical feedback mechanism in the laser is necessary to keep the process of stimulated emission going. The optical feedback is provided by the cleaved facets at both ends of the device, acting as

partially transparent mirrors, see Fig. 2.1. These mirrors form a so called Fabry-Perot cavity in which the light is reflected back and forth through the active region, resulting in standing waves inside the laser cavity. For simplicity, the standing waves will be descibed as a plane wave propagating in the positive z-direction [3]. If the z-axis is taken along the cavity length, the optical field of the plane wave in the cavity can be described as

$$E = E_0 \, \mathrm{e}^{\mathrm{i}\beta z} \tag{2.1}$$

where E_0 is the constant amplitude and β is the complex propagation constant which is defined as

$$\beta = nk_0 \; + \; \frac{i\alpha}{2} \tag{2.2}$$

Here n is the refractive index, $k_0 = \omega/c = 2\pi/\lambda$ is the wavenumber and α is the power absorption coefficient. From Eq. (2.1) and Eq. (2.2) it is clear that the propagation characteristics of the plane wave can be described with the two important optical parameters, n and α.

The refractive index is determined by the composition of the material and changes if a current is injected. The absorption coefficient is given by

$$\alpha = -\Gamma g + \alpha_{\mathrm{int}} \tag{2.3}$$

where g is the net gain and α_{int} represents the internal losses, which are due to free-carrier absorption and scattering at the borders of the active layer. Γ is the confinement factor and represents the fraction of power propagating in the active section.

To obtain the threshold condition, the net change in amplitude after one round trip time must be zero. The distance that the plane wave covers in one round trip time is two times the cavity length. At the end facets of the cavity only part of the light is reflected back into the cavity. The threshold condition can described as, see Eq. (2.1),

$$\sqrt{R_1 R_2} \;\; \mathrm{e}^{2i\beta L_{\mathrm{cav}}} = 1 \tag{2.4}$$

where R_1 and R_2 are the facet power reflectivities. This condition can be separated into two conditions by equating the real and imaginary parts of Eq. (2.4) and substituting β from Eq. (2.2)

$$\sqrt{R_1 R_2} \;\; \mathrm{e}^{-\alpha L_{\mathrm{cav}}} = 1 \tag{2.5}$$

$$\sin(2nk_0 L_{\mathrm{cav}}) = 0 \tag{2.6}$$

The first condition, Eq. (2.5), is the gain condition and it is met if the round trip gain in the cavity is equal to one. This is the case if the gain in the laser equals the total loss, being the internal loss within the cavity and the mirror loss (i.e. the loss due to the emitted light). The threshold gain is then

$$\Gamma g = \alpha_{\mathrm{m}} \; + \; \alpha_{\mathrm{int}} \tag{2.7}$$

where

$$\alpha_m = \frac{1}{2L_{cav}} \ln(\frac{1}{R_1 R_2}) \tag{2.8}$$

is the mirror loss.

The second condition, Eq. (2.6), is the phase condition which can be used to obtain the lasing frequency,

$$2nk_0 L_{cav} = 2m\pi \tag{2.9}$$

where m is an integer. Using $k_0 = 2\pi/\lambda$ the lasing wavelength is given by

$$\lambda_m = \frac{2nL_{cav}}{m} \tag{2.10}$$

where λ_m is the wavelength of the m-th longitudinal mode of the FP cavity. Equation (2.10) shows that the laser tends to oscillate at wavelengths which fit in the FP cavity with optical length nL_{cav}. Which one and how many of them reach threshold depends on the gain profile. The left side of Fig. 2.2 schematically shows the gain profile, the loss in the cavity and the longitudinal modes. In the vicinity of the gain peak the modes can reach threshold (where the gain equals the loss).

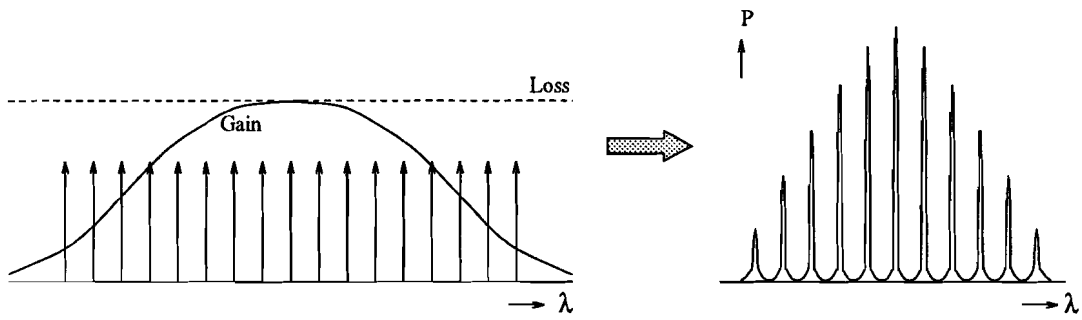

Figure 2.2: **Schematic illustration of the gain profile, loss and longitudinal modes of a semiconductor laser. The right part of the figure shows the resulting power spectrum.**

The separation between two longitudinal modes can be obtained from Eq. (2.10) by

$$\Delta\lambda = \frac{\lambda^2}{2nL_{cav}} \tag{2.11}$$

From Eq. (2.11) it follows that $\Delta\lambda$ becomes very small if the cavity length becomes large. As a result, many modes can reach threshold, leading to a multimode spectrum, see Fig. 2.2.

The light in a semiconductor laser should be confined to the thin active region because

this region provides the opical gain. In the laser depicted in Fig. 2.1, the so-called double-heterostructure laser, the light is confined in the transverse direction, perpendicular to the junction plane, because the cladding layers have a lower index of refraction compared to that of the active region. This results in total internal reflection of the light and thus confinement of the light in the transverse direction. In the lateral direction, along the junction plane, there is no confinement of the light, resulting in multi lateral modes. Furthermore, due to the large width of the laser, the total current required for lasing operation becomes rather high. It is often desirable to design semiconductor laser that emit light predominantly in a single lateral mode, because important laser characteristics such as the near- and far-field depend on the number of modes. For semiconductor lasers the far-field distribution plays an important role as it determines the amount of power coupled into a fiber. The confinement of the light in the lateral direction and the reduction of current can be improved using, for example, a Semi Insulating Planar Burried Heterostructure laser (SIPBH), see Fig. 2.3. The semi insulating blocking layers (InP:Fe) are highly resistive and therefore the current can flow only through the gap between the blocking layers, resulting in a reduced current. The blocking layers also have a lower index of refraction than the active section, resulting in confinement of the light in the lateral direction as well.

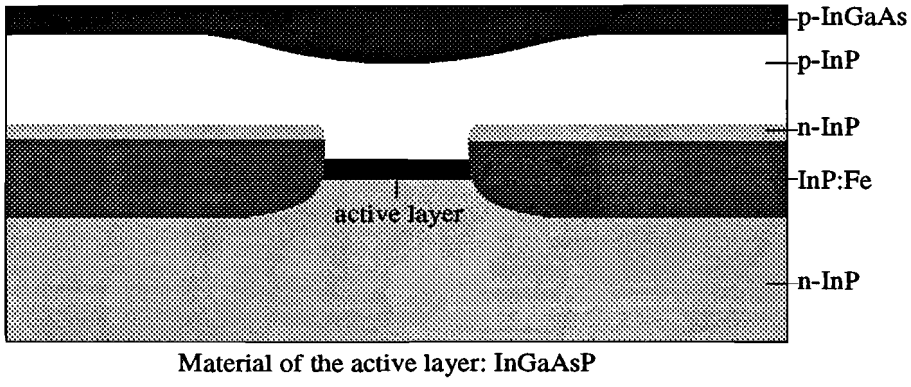

Figure 2.3: **Cross-section of a Semi Insulating Planar Burried Heterostructure laser.**

2.2 The tunable 3-section Distributed Bragg Reflector laser.

A single-frequency laser can be obtained by replacing one mirror facet by a frequency selective mirror, e.g. a grating, see the inset of Fig. 2.4. The grating region is outside the active region along the length of the cavity and is called a Distributed Bragg Reflector (DBR). The DBR section reflects only a small wavelength range around the Bragg wavelength λ_{bragg}, see Fig. 2.4. The Bragg wavelength λ_{bragg} is related to the period of the

grating Λ by

$$\lambda_{\text{bragg}} = \frac{2n_e\Lambda}{m} \tag{2.12}$$

where n_e is the effective refractive index and m is the order of Bragg diffraction induced by the grating. The Bragg gratings which are fabricated nowadays almost invariably have $m = 1$, which gives best performance. In Fig. 2.4 are drawn also some wavelength peaks which fulfil the solutions of the phase condition of Eq. (2.10). The mode at the Bragg wavelength, which has the highest reflectivity and thus the lowest loss and threshold gain, will lase predominantly.

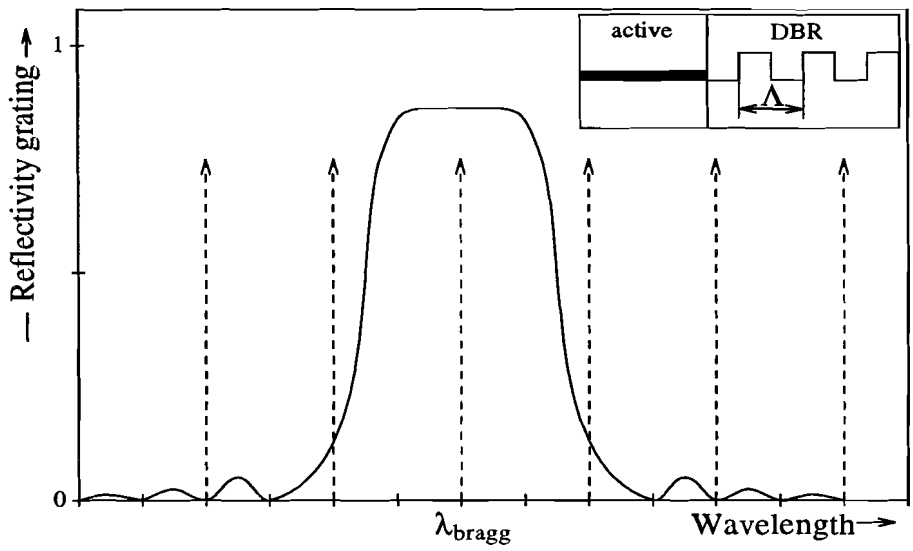

Figure 2.4: **The selection of a wavelength by means of a Bragg reflector. The solid line shows the reflectivity of the Bragg section and the dashed lines are solutions of the phase condition. The inset shows a DBR laser with a period Λ of the grating.**

When current is injected into the Bragg region, the carrier density increases and simultaneously the effective refractive index n_e decreases due to the free-carrier plasma effect, resulting in a decrease of the Bragg wavelength, see Eq. (2.12). By injecting a current into the DBR region it is thus possible to shift the main lobe of the reflectivity to lower wavelengths. At the same time, the wavelengths which fulfils the phase condition shift to lower wavelengths. However, this shift is small compared to the shift in Bragg wavelength. When the shift in Bragg wavelength is large enough, a mode jump occurs to the adjacent lower wavelength which fulfils the phase condition. The result is a discontinuous wavelength tuning. By adding a third section (Phase Control section) between the gain section and the DBR section, see Fig. 2.5, quasi continuous wavelength tuning can be obtained. This laser is called a tunable three-section DBR laser. When current is injected into the Phase

Control (PC) section the phase matching condition of the waves in the gain section and the DBR section is changed. This leads to a shift in the wavelengths of the longitudinal modes, see Eq. (2.10). The result in Fig. 2.4 is the shift of the wavelength peak over the main lobe of the reflectivity. By changing the PC and DBR currents at the same time it is possible to get a continuous tuning characteristic.

To get a better insight into the tunable 3-section DBR laser the model of [1] is presented briefly in this report. This model describes the tunable 3-section DBR laser, which is analogous to the description of the semiconductor laser given in section 2.1.

2.2.1 Theoretical model of the 3-section DBR laser.

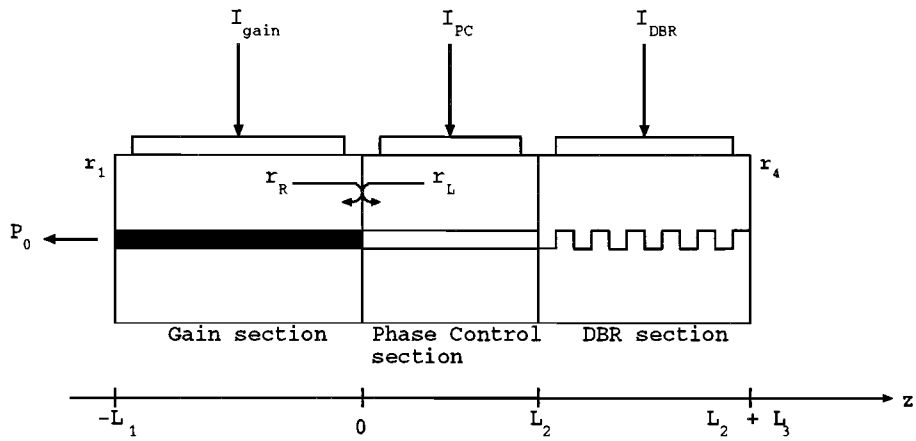

Figure 2.5: Schematic diagram of a tunable three-section Distributed Bragg Reflector laser.

Figure 2.5 shows a schematic diagram of a tunable three section Distributed Bragg Reflector laser. The laser has three sections: an active section for light generation and control of the output power and a DBR section for selection of the longitudinal mode. The PC section takes care of phase matching of light waves in the DBR section and the gain section. The three sections of the laser have separate electrodes and are assumed to be electrically isolated from each other. The PC and DBR section are made of higher bandgap material than the active section and therefore are transparent at the lasing wavelength.

The theoretical analysis is based on a transmission line theory for compound cavity semiconductor lasers [4]. For simplicity the possible reflections at the interface between the gain section and the PC section are neglected. The reflectivity of the right facet of the DBR section is also neglected, $r_4 = 0$. A reference plane is considered in Fig. 2.5 at $z = 0$.

The effective reflection coefficient for the left going electric field is given, at this plane, by:

$$r_{\mathrm{L}}(\omega, S, N_1) = r_1 e^{-2jL_1 k_1(\omega, S, N_1)} \tag{2.13}$$

where r_1 is the reflectivity at the left facet ($z = -L_1$), N_1 is the carrier density in the active section, S is the photon number in the laser cavity, ω is the angular frequency of the lasing field and k_1 is the wavenumber, given by :

$$k_1(\omega, S, N_1) = \frac{\omega n_1(\omega, S, N_1)}{c} + \frac{j}{2}[g(S, N_1) - \alpha_1] \tag{2.14}$$

where c, n_1, g and α_1 are the light velocity, the refractive index, the modal gain and the internal loss per unit length, respectively. The modal gain is given by:

$$g(S, N_1) = a_1(N_1 - N_0) \tag{2.15}$$

where a_1 is the gain coefficient and N_0 the carrier density at transparency. From Eq. (2.15) it is observed that the gain increases when the carrier density, and thus the injection current, increases.

The effective reflectivity r_{R} for the right going field at the reference plane is given by:

$$r_{\mathrm{R}}(\omega, N_2, N_3) = r_{\mathrm{DBR}}(\omega, N_3) e^{-2jk_2(\omega, N_2)L_2} \tag{2.16}$$

In Eq. (2.16) N_2 and N_3 are the carrier densities in the PC and DBR sections, respectively, and r_{DBR} represents the reflectivity of the DBR section, given by [5]:

$$r_{\mathrm{DBR}}(\omega, N_3) = \frac{e^{j\Phi}}{j} \; \frac{\frac{\kappa}{\hat{\Gamma}}(\rho - \frac{\hat{\Gamma}}{\kappa})e^{\epsilon L_3} + \frac{\hat{\Gamma}}{\kappa}(\frac{\kappa}{\hat{\Gamma}} + \rho)e^{-\epsilon L_3}}{(\frac{\hat{\Gamma}}{\kappa} - \rho)e^{\epsilon L_3} + (\frac{\kappa}{\hat{\Gamma}} + \rho)e^{-\epsilon L_3}} \tag{2.17}$$

where

$$\rho = jr_3 e^{-j(2\beta_0 L_3 + \Phi)} \tag{2.18}$$

$$\epsilon = \sqrt{\kappa^2 - [k_3(\omega, N_3) - \beta_0]^2} \tag{2.19}$$

$$\hat{\Gamma} = -\epsilon - j[k_3(\omega, N_3) - \beta_0] \tag{2.20}$$

and β_0 is the Bragg propagation constant, κ is the coupling coefficient, r_3 is the facet reflectivity at the end of the DBR section ($z = L_2 + L_3$) and Φ is the corrugation phase at $z = L_2$.

The wavenumbers for the passive sections are given by:

$$k_i(\omega, N_i) = \frac{\omega n_i(\omega, N_i)}{c} - \frac{j\alpha_i(N_i)}{2} \qquad i = 2, 3 \tag{2.21}$$

where

$$n_i(\omega, N_i) = n_0 + \Gamma \frac{dn_i}{dN_i} N_i \qquad i = 2, 3 \tag{2.22}$$

$$\alpha_i(N_i) = \alpha_0 + \Gamma \frac{d\alpha_i}{dN_i} N_i \qquad i = 2,3 \tag{2.23}$$

n_0 and α_0 being the refractive index and the internal absorption in the absence of carrier injection, Γ the confinement factor, dn_i/dN_i and $d\alpha_i/dN_i$ the parameters describing the free-carrier plasma effect and the free-carrier absorption, respectively. The carrier densities in the passive sections are related to the injection currents by:

$$I_{\mathrm{PC}} = eV_2R(N_2) \tag{2.24}$$

$$I_{\mathrm{DBR}} = eV_3R(N_3) \tag{2.25}$$

where e is the electron charge, V_2 and V_3 are the waveguide volumes of the PC and DBR sections, respectively, and $R(N_i)$ is the total spontaneous recombination rate per unit volume, given by:

$$R(N_i) = c_1N_i + c_2N_i^2 + c_3N_i^3 \qquad i = 2,3 \tag{2.26}$$

c_1, c_2, c_3, being constants. The recombination constant c_3 accounts for Auger recombination.

Figure 2.6 illustrates the behaviour of the reflectivity of the DBR section at a number of DBR currents as calculated from Eq. (2.17). The parameters used to describe the DBR section in this calculation are listed in the table of Fig. 2.6. If the DBR current increases, the carrier density in the DBR section increases, see Eq. (2.25) and Eq. (2.26). The result is a decrease in the refractive index, see Eq. (2.22) (dn_i/dN_i is negative) which leads to a shift of the Bragg wavelength to shorter wavelengths. Furthermore an increasing DBR current result in an increase in the absorption, see Eq. (2.23) ($d\alpha_i/dN_i$ is positive) which leads to a lower reflectivity, as observed in Fig. 2.6.

The oscillation condition for the laser is:

$$r_{\mathrm{L}}(\omega, S, N_1) \cdot r_{\mathrm{R}}(\omega, N_2, N_3) = 1 \tag{2.27}$$

This oscillation condition can be separated into two conditions, one for the gain and one for the phase shift of the field during one round-trip in the total cavity. The gain condition is found from the norm of equation 2.27:

$$\ln |r_{\mathrm{L}} r_{\mathrm{R}}| = 0 \tag{2.28}$$

The phase condition is:

$$h(\omega) = 2\pi p, \qquad \text{p integer} \tag{2.29}$$

where

$$h(\omega) = 2\frac{\omega}{c} n_1(\omega, N_1)L_1 + 2\frac{\omega}{c} n_2(\omega, N_2)L_2 - \arg[r_{\mathrm{DBR}}(\omega, N_3)] \tag{2.30}$$

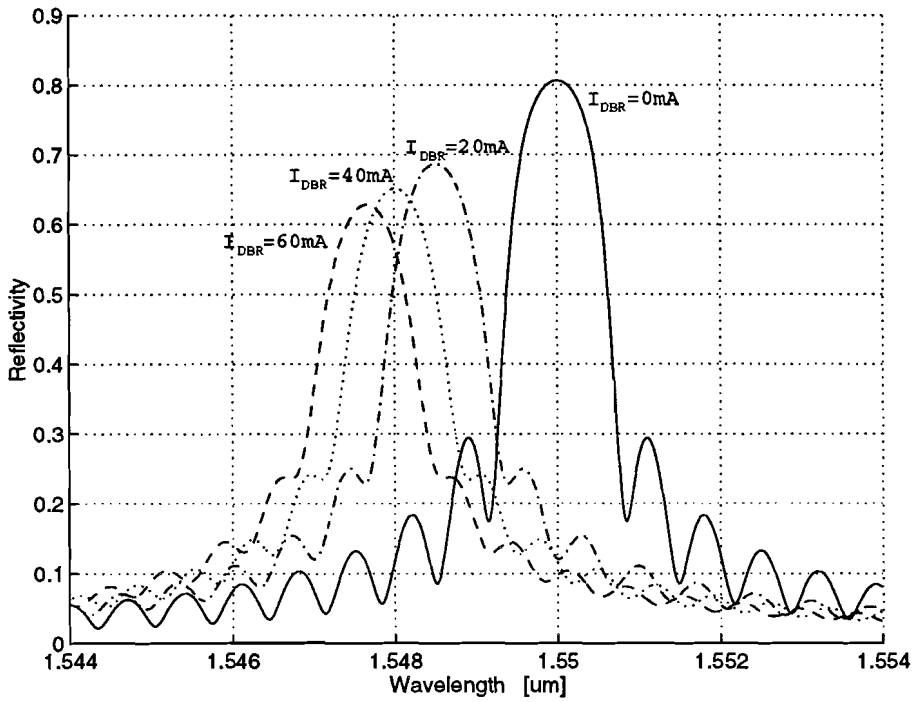

Parameter	Symbol	Value	Unit
Refractive index	n_0	3.4	
Confinement factor	Γ	0.3	
Recombination coefficient	c_1	$1 \cdot 10^{8}$	s^{-1}
Recombination coefficient	c_2	$8 \cdot 10^{-17}$	m^3/s
Recombination coefficient	c_3	$4 \cdot 10^{-41}$	m^6/s
Index derivative with repsect to carrier density	$\frac{dn}{dN}$	$-6 \cdot 10^{-27}$	m^3
Absorption derivative with repsect to carrier density	$\frac{d\alpha}{dN}$	$26 \cdot 10^{-22}$	m^2
Internal absorption	α_0	20	cm^{-1}
Bragg wavelength	λ_{bragg}	1.55	μm
Width of waveguide layers	W	1	μm
Thickness of waveguide layers	D	0.25	μm
Length of PC section	L_2	100	μm
Length of DBR section	L_3	500	μm
Facet reflectivity at the end of the DBR section ($z = L2 + L3$)	r_4	0	
Corrugation phase	Φ	0	rad
Normalised coupling coefficient	κL_3	2	

Figure 2.6: **Reflectivity of the Bragg section at a number of DBR currents. The parameters used to describe the DBR section are listed in the table.**

As shown in [4], the function can be approximated by the following expression:

$$h(\omega) = h_0 + \omega\tau_{\text{in}} + 2\frac{\omega}{c}n_2 L_2 + \beta \ln|r_{\text{DBR}}| - \arg(r_{\text{DBR}}) \tag{2.31}$$

where h_0 is a parameter which only depends on the internal state of the active section, $\tau_{\text{in}} = 2L_1/v_g$ is the roundtrip time in the active cavity, v_g is the group velocity and β is the material value of the linewidth enhancement factor.

From the gain and phase conditions, Eq. (2.28) and (2.30), it is possible to calculate the lasing wavelength of the dominant mode when the PC and DBR currents are changed [1], see Fig. 2.7. As the current into the DBR region increases, the Bragg wavelength decreases (see Eq. (2.22) and the dashed line in Fig. 2.7) and causes mode-hopping among the longitudinal modes in the DBR laser cavity, see Fig. 2.7a. When the PC current is changed at a fixed DBR current the wavelength is tuned over the main lobe of the Bragg reflector, as illustrated in Fig. 2.7b. The wavelength is decreasing between the mode jumps and mode jumps become less frequent as I_{pc} is increased. When I_{DBR} increases, the mode jumps become also less frequent. This is due to saturation of the carrier density N_2 and N_3 at high injection level. By changing both of the two currents to the passive sections at the same time it is possible to obtain continuous tuning over a large wavelength range.

The output power from the front facet at the left in Fig. 2.5 is:

$$P_0 = \hbar\omega\eta_i S v_g (g_{\text{th},1} - \alpha_1)\frac{(1-r_1^2)|r_{\text{R}}|}{(1-r_1|r_{\text{R}}|)(r_1+|r_{\text{R}}|)} \tag{2.32}$$

where the photon number in the gain section S is given by

$$S = \frac{I_{\text{gain}}}{e g_{\text{th},1} V_1} \tag{2.33}$$

and η_i is the internal quantum efficiency and $\hbar$ is Planck's constant divided by 2π. $g_{\text{th},1}$ is the threshold gain and V_1 is the volume of the active layer. P_0 is drawn in figure 2.7 as a function of the PC and DBR current by the dotted line. The output power P_0 shows a decreasing trend because of the increase of free-carrier absorption in the passive sections, see Eq. (2.23) ($d\alpha_i/dN_i$ is positive). Comparing Fig. 2.7a and 2.7b, we see that the output power is more sensitive to I_{PC} than to I_{DBR}.

In the previous model it is assumed that the PC and DBR sections are made of larger bandgap material than the active section, and therefore are transparent at the lasing wavelength. With increasing tuning current, free-carrier absorption in these sections results in a decreasing output power. If the PC and DBR section are made of material with a bandgap that is close to that of the active section, the PC and DBR section can deliver

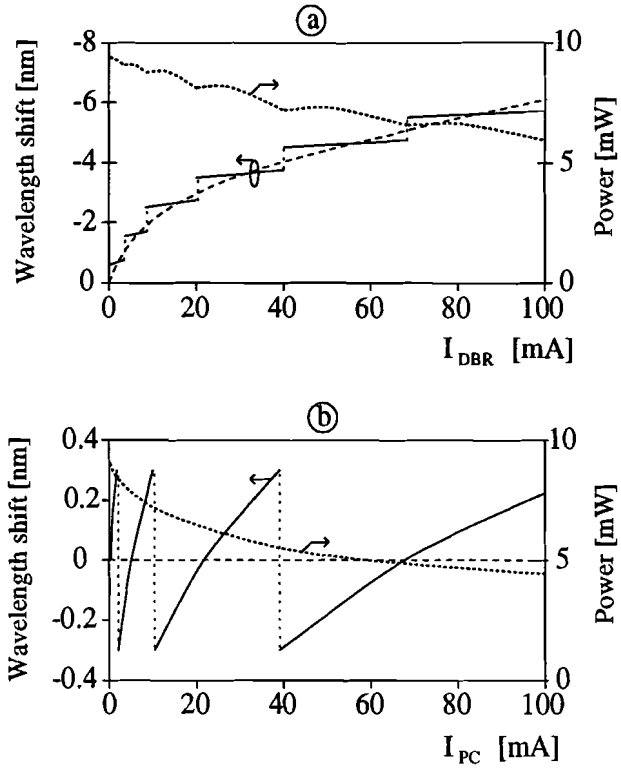

Figure 2.7: **Tuning and power characteristics as a function of DBR current and PC current. The dashed line shows the shift in Bragg wavelength. (After Ref. [1])**

some amplification with increasing PC and DBR current [2]. This can be taken into account in Eq. (2.26) by adding a term describing the stimulated emssion occuring in these sections:

$$R(N_i) = c_1 N_i + c_2 N_i^2 + c_3 N_i^3 + R_{\mathrm{st},i}\, S \qquad i = 2,3 \tag{2.34}$$

where

$$R_{\mathrm{st},i} = \frac{c}{n_{\mathrm{g}}}\, g_i(N_i) \qquad i = 2,3 \tag{2.35}$$

with $g_i(N_i)$ the optical gain in the PC and DBR section, respectively. If the DBR and PC currents increase, both the gain (Eq. (2.35)) and the absorption (Eq. (2.23)) increase. The amount of these increases depends on material parameters, such as the bandgap, and leads to a positive or negative net gains (gain minus absorption).

3. Static properties

3.1 Measurement setup

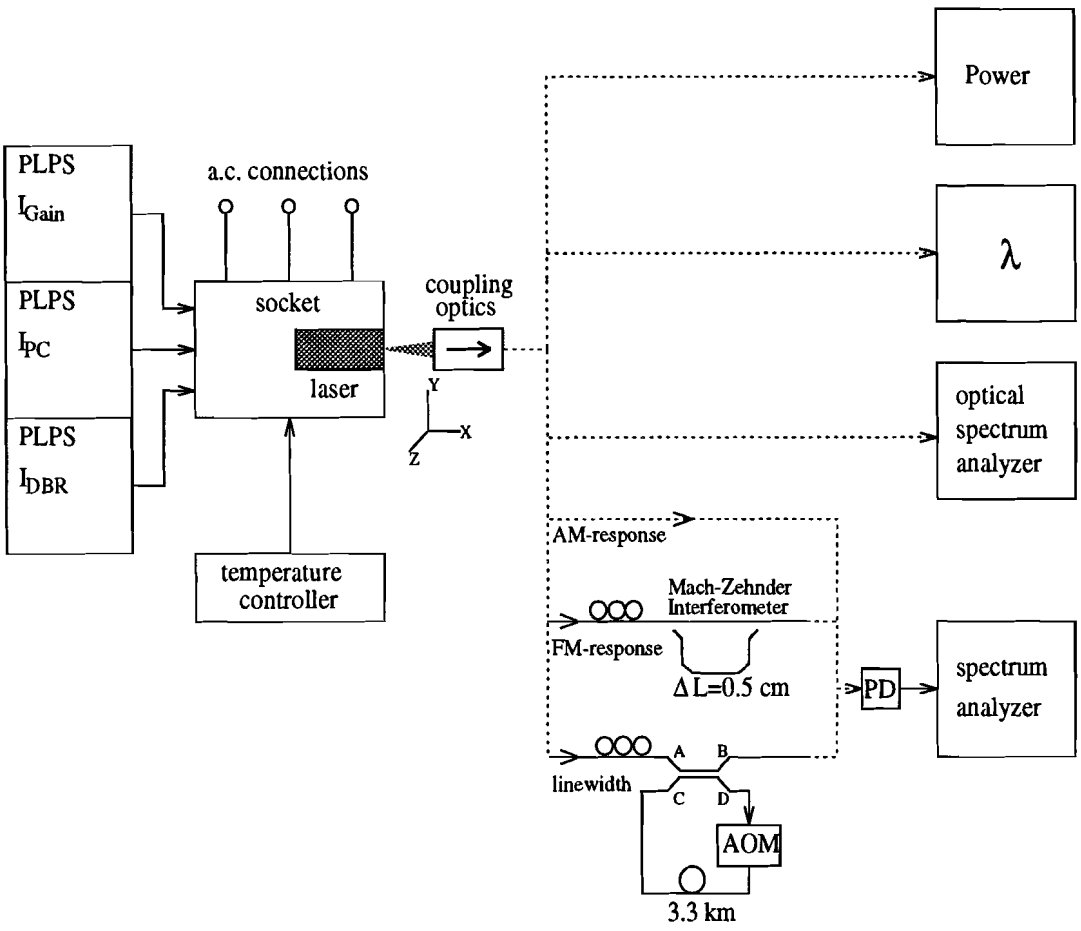

Figure 3.1: Measurement setup.

For the measurements of the static and dynamic properties of the 3-section DBR laser the measurement setup shown in Fig. 3.1 is used. The laser is mounted in a socket which is held at a constant temperature using a Peltier element. The three bias currents, I_{gain}, I_{PC} and I_{DBR}, are adjusted by the three current supplies (PLPS). The light from the laser is coupled into a single mode fiber by the coupling optics, including an optical isolator which transmits the light from the laser to the optical fiber but prevents the reflected light from returning to the laser. This is necessary because light that is coupled back into the

laser generates noise in the laser output, disturbing its laser spectrum. In the measurement setup various connections can be made to measurement instruments, such as a power meter, wavelength meter and an optical spectrum analyzer. The three lowest connections are used for measuring of the AM response, FM response, and linewidth, respectively. The measurements of the dynamic properties (AM and FM response) and of the linewidth are explained respectively in chapter 4 and section 3.5.

The lasers in table 3.1 are available for measurements:

Wafer no.	Technology no.	Λ [Å]	Bandgap	Coating gain section	
MOQT2775-1	LD1632	2402	$Q_{1.45}$ WG	-	
MOQT2775-2	LD1634	2402	$Q_{1.48}$ WG	-	
MOQT2776-1	LD1636	2410	$Q_{1.45}$ WG	-	
MOQT2776-1	LD1636	2410	$Q_{1.45}$ WG	10%	
MOQT2776-2	LD1638	2410	$Q_{1.48}$ WG	-	
MOQT2777-1	LD1640	2410	$Q_{1.45}$ WG	-	8 SL-QW
MOQT2777-1	LD1640	2410	$Q_{1.45}$ WG	10%	8 SL-QW
MOQT2777-2	LD1642	2410	$Q_{1.48}$ WG	-	8 SL-QW
MOQT2779-1	LD1644	2418	$Q_{1.45}$ WG	-	
MOQT2779-2	LD1646	2418	$Q_{1.48}$ WG	-	

Table 3.1: Lasers available for measurements.

The lasers have a SIPBH structure as described in chapter 2.1. Some of the lasers contain quantum wells in the active layer, e.g. MOQT2777-1 and MOQT2777-2 (8 SL-QW means that there are 8 Strained Layer Quantum Wells in the active layer). In general, the use of quantum wells leads to a higher output power, a reduced threshold current and a narrow linewidth [3].

The wavelength of a DBR laser is determined by the Bragg wavelength, which in turn is determined by the pitch of the grating Λ and the effective refractive index, see Eq. (2.12). During fabrication, there are variations in the production proces, resulting in variations of the parameters. Especially the effective refractive index is difficult to predict and therefore also the exact wavelength of the laser. A spread in wavelength within a single wafer of about 2 nm is normal. For this reason a series of lasers is made, and each series has a different pitch of the grating in the DBR section, see table 3.1. Then the laser with the desired wavelength can be selected from the laser series.

$Q_{1.45}$ WG means that in the PC and DBR sections a waveguide of quaternary material composition (InGaAsP) is used with a bandgap wavelength of 1.45 μm. The $Q_{1.48}$ WG has a bandgap wavelength of 1.48 μm. The bandgap wavelengths are varied slightly, to examine the bandgap dependency of the flatness of the power characteristic of the different wafers, see section 3.3.

In the previous chapter, zero reflectivity has been assumed on the facet of the DBR section (i.e. $r_4 = 0\%$). The reflectivity of an as-cleaved facet is about 30 % which would result in spurious Fabry-Perot resonances. Therefore an Anti-Relection coating (AR) is applied on the back facet (DBR section) of all the lasers to reduce this effect. No coating is applied on the front facet (gain section) of the laser, except for some lasers of MOQT2776-1 and MOQT2777-1, which received a 10 % coating. These lasers have been used for wavelength conversion experiments as described in Chapter 5.

3.2 Tuning characteristic

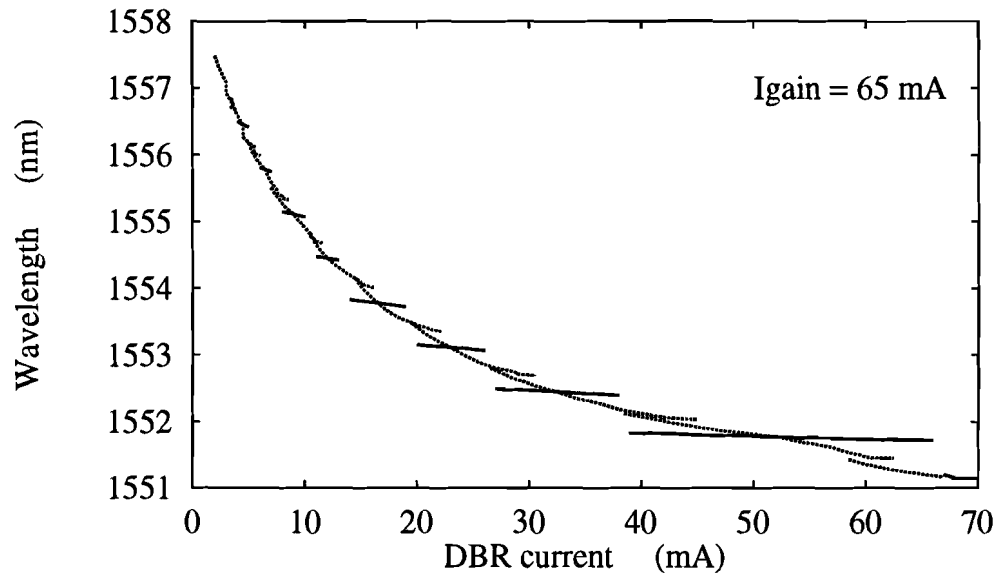

Figure 3.2: **Tuning characteristic of a 3-section DBR laser. The solid lines show the wavelength as a function of the DBR current with a constant PC current. The dotted line shows the quasi continuous wavelength tuning when both the DBR current and the PC current are controlled.**

Figure 3.2 shows a tuning characteristic of a 3-section DBR laser. When a constant PC current is applied, the wavelength tuning as a function of the Bragg current occurs by mode hopping, see the solid line in Fig. 3.2. Each successive mode has a shorter wavelength than the previous one. Within a single mode, continuous tuning is accomplished by varying the phase current and, in order to keep track of the mode, by simultaneously varying the Bragg current as well, since the modes shift towards larger Bragg currents with increasing PC current. The result is a quasi continuous tuning curve of approximately 6 nm, see the dotted line in Fig. 3.2. Typical values of the DBR and PC current are 0-70 mA and 0-30 mA, respectively.

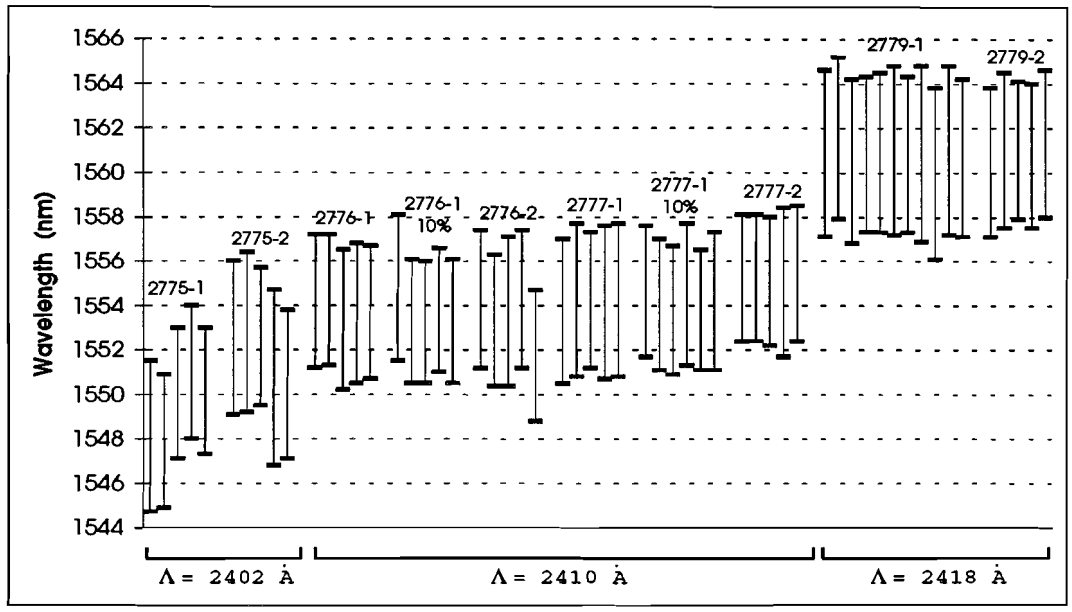

Figure 3.3: Wavelength ranges for a few lasers of the 8 different wafers.

In Fig. 3.3 the wavelength ranges are drawn for a few lasers of the 8 wafers. The wavelength ranges for all wafers are about 6 nm, and shift to higher wavelengths when the pitch of the grating Λ increases. The spread in central wavelengths is for MOQT2775-1, MOQT2775-2 and MOQT2776-2 about 4 nm, the others exhibit a spread of about 2 nm. As an example, the tuning characteristics of 5 lasers of MOQT2775-2 are given in Fig. 3.4. Here, it is observed that the spread in central wavelengths of 4 nm splits into two groups, each having a spread of less than 1 nm. It appears that there are two Bragg wavelengths in the wafer, which might be due to variations in the effective-mode index or the pitch of the grating.

3.3 Power characteristic

The next important characteristic is the power characteristic. This curve preferably must be as flat as possible over the entire tuning range. The flatness of the power characteristic depends on the bandgap in the PC and DBR section, see Chapter 2.2.1. To examine the bandgap dependency of the flatness of the power-characteristic, the bandgaps in the PC and DBR section of the different wafers are varied slightly, see table 3.1. In Fig. 3.5 curves are drawn for two lasers with different bandgaps in the PC and DBR section. With increasing tuning current (decreasing wavelength) too much amplification leads to an increasing power curve in each single mode, and insufficient amplification results in a decreasing power curve in each single mode, see Fig. 3.5.

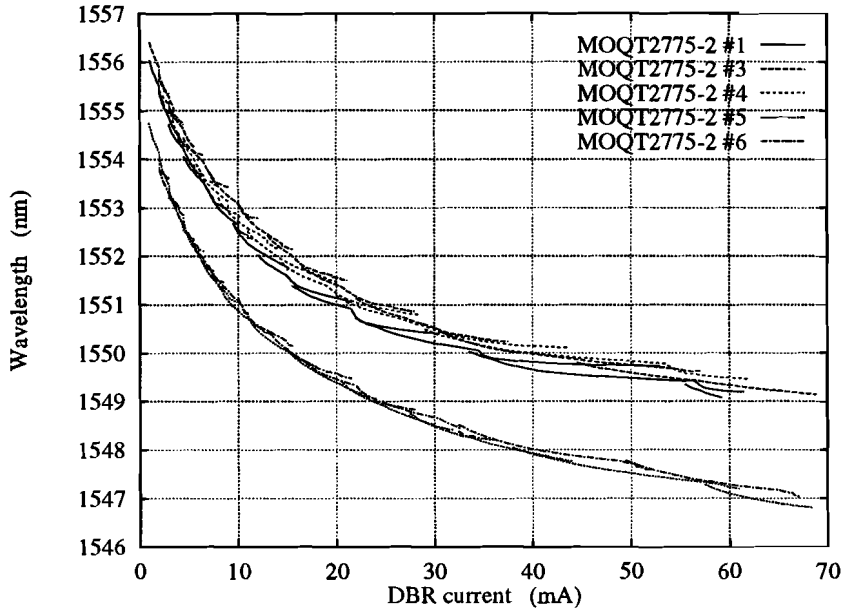

Figure 3.4: Tuning characteristics of 5 lasers of MOQT2775-2.

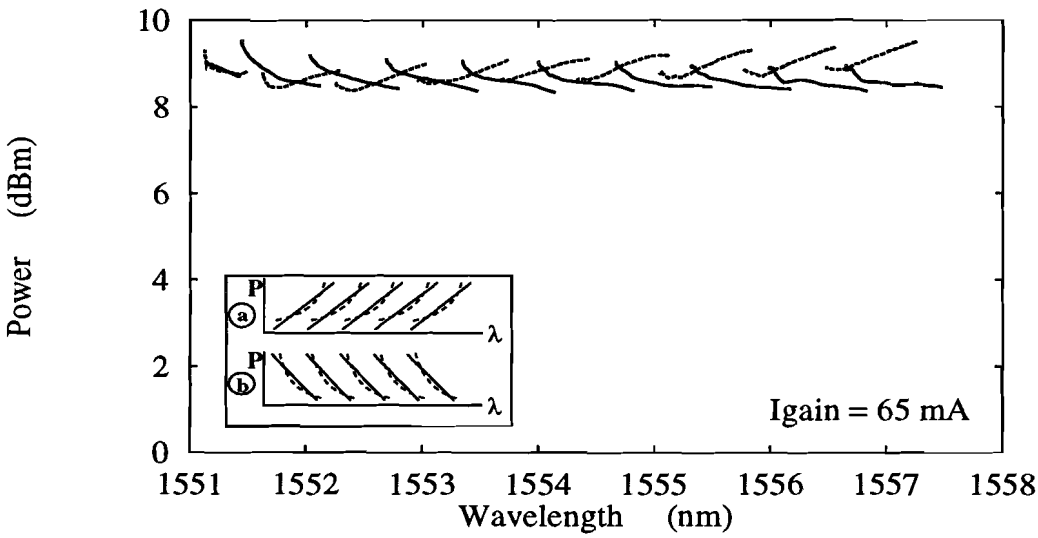

Figure 3.5: Power charateristic of two lasers. The solid line is a $Q_{1.48}$ laser and the dotted line is a $Q_{1.45}$ laser. The inset shows the power characteristic of the two laser with lines through each mode. The overlapping parts of the modes in each power characteristic are removed to get a improved flatness of the curve.

In Fig. 3.6 and Fig. 3.7 the $P(I_{\mathrm{DBR}})$ and $P(I_{\mathrm{PC}})$ curves are drawn for a $Q_{1.45}$ and a $Q_{1.48}$ laser, respectively. The jumps in the $P(I_{\mathrm{DBR}})$ and $P(I_{\mathrm{PC}})$ curves are due to mode jumps. The decrease in power in one mode of the $P(I_{\mathrm{DBR}})$ curve is indentical for the $Q_{1.45}$ and the $Q_{1.48}$ lasers. The decrease in power in a mode, as a result of the increase of the DBR current, can be compensated by the increase in power in a mode if the PC current is increased. The increase in power in the $P(I_{\mathrm{PC}})$ curve in a mode is larger for the $Q_{1.48}$ laser and therefore it can deliver more compensation than the $Q_{1.45}$ laser.

When the DBR current increases the main lobe of the reflectivity shifts to lower wavelengths while the lasing wavelength approximately remains the same. The result is a decrease in the reflectivity, see Fig. 3.8, leading to a decrease in the output power in a mode.

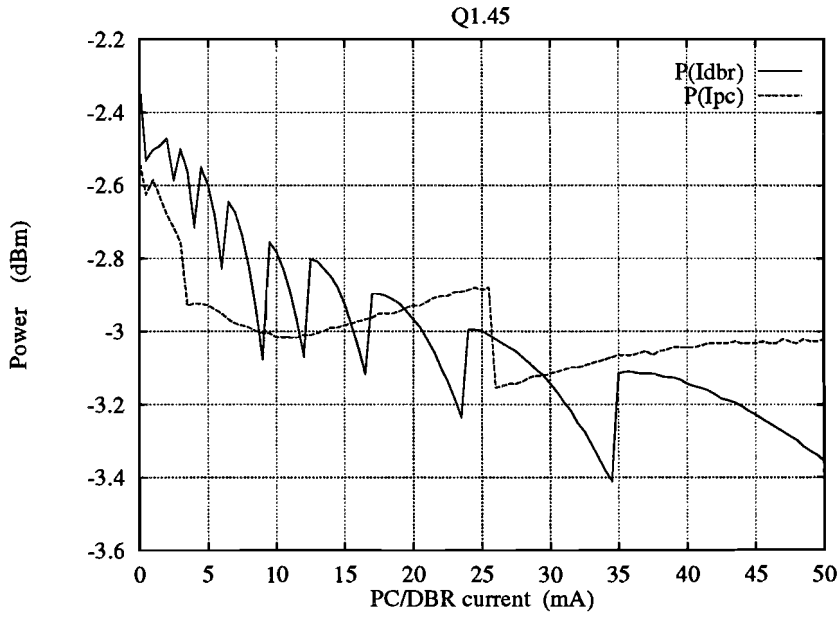

Figure 3.6: Output power as a function of the PC and DBR currents for a $Q_{1.45}$ laser.

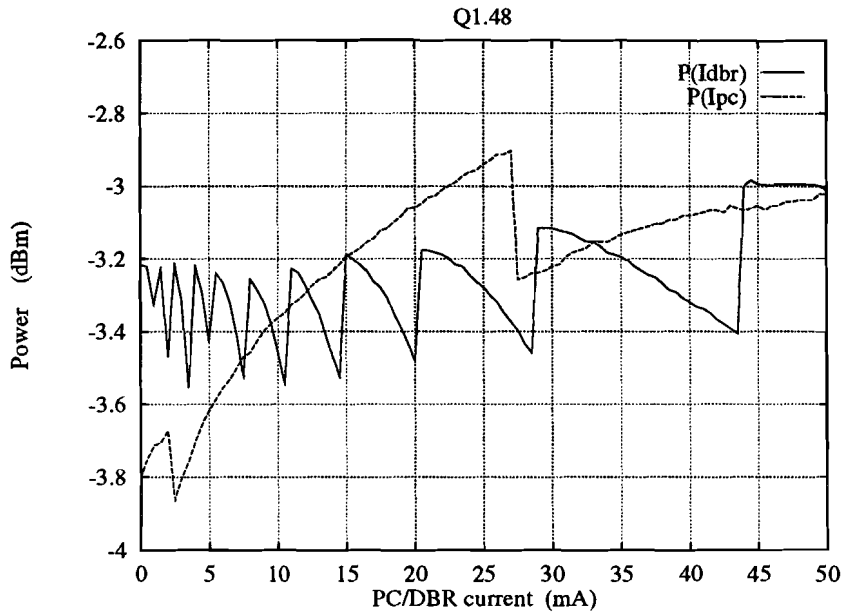

Figure 3.7: **Output power as a function of the PC and DBR currents for a $Q_{1.48}$ laser.**

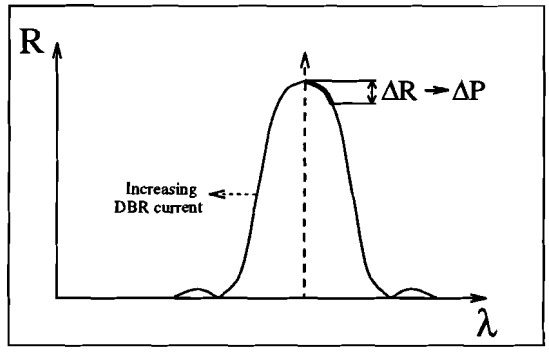

Figure 3.8: **Illustration of the decrease in reflectivity and power in a mode when the DBR current increases.**

To explain the shape of the $P(I_{PC})$ curve, transmission measurements of the PC section are made, using the measurement setup of Fig. 3.9. The gain section is cleaved off from the laser. The output power is measured for varying the input wavelength while the input power is held constant at -10 dBm. In Fig. 3.10 and Fig. 3.11 the output power is drawn for the $Q_{1.45}$ and the $Q_{1.48}$ laser at two values of the PC current. These figures shows a minimum, as a result of the wavelength dependent reflectivity of the DBR section. The transmitted power increases in the case of a $Q_{1.48}$ waveguide layer (outside the reflectivity band of the DBR), while it remains constant for a $Q_{1.45}$ layer. This is in agreement with the $P(I_{PC})$ curves shown in Fig. 3.6 and 3.7.

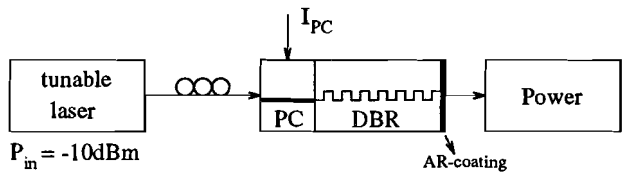

Figure 3.9: **Measurement setup to measure $P_{out}(\lambda)$ for different I_{PC}. The gain section is cleaved off from the laser. Light is coupled into and out the laser by fiber tips.**

The values of the transmitted powers in Fig. 3.10 and 3.11 can not easily compared, because of the different coupling efficiencies. However, due to the larger absorption in the $Q_{1.48}$ layer, one expects the transmitted power to be less than for a $Q_{1.45}$ layer (in the case of equal coupling efficienties).

Fig. 3.10 and 3.11 show oscillations outside the reflectivity band of the DBR, which are the result of the FP cavity, formed by the facets. The length of this cavity can be calculated from the period of the oscillations ($\Delta\lambda = 0.55$ nm), using Eq. (2.11), and results in $L_{cav} = 642$ μm where an effective refractive index of 3.4 is assumed. The length of the laser, without the gain section, is 600 μm, which agrees well with the measurement.

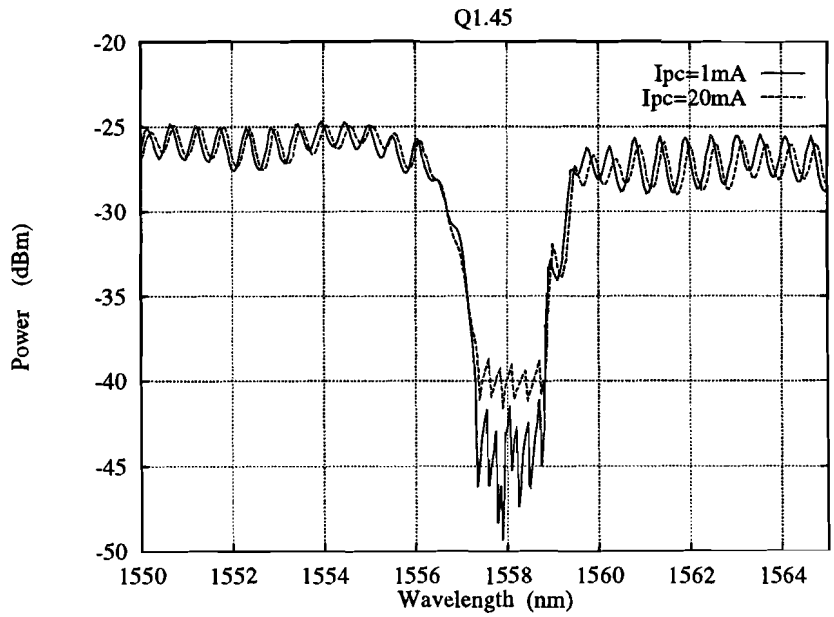

Figure 3.10: Output power as a function of the wavelength for 2 different PC currents. The laser has a $Q_{1.45}$ waveguide layer in the tuning sections.

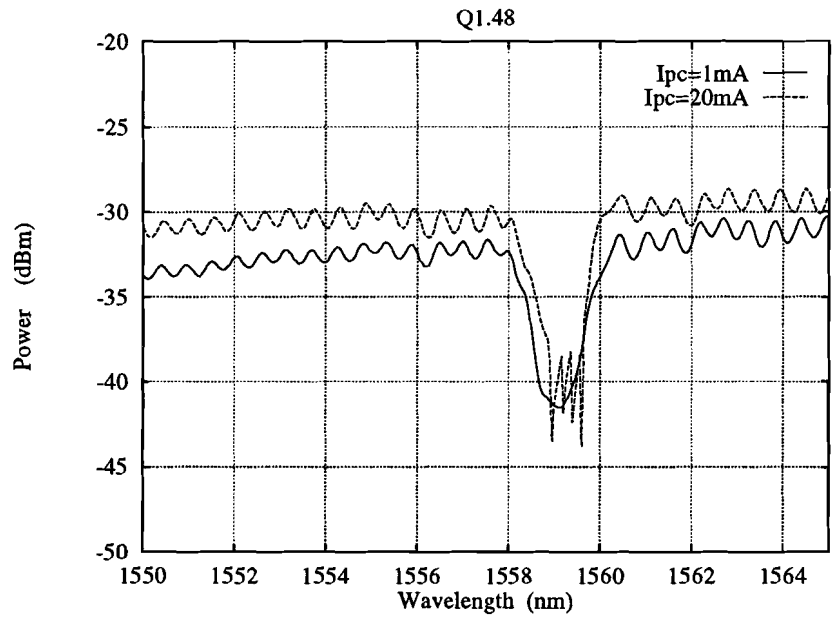

Figure 3.11: Output power as a function of the wavelength for 2 different PC currents. The laser has a $Q_{1.48}$ waveguide layer in the tuning sections .

In order to determine which bandgap is the best in the PC and DBR sections the power characteristics have been measured for a few lasers of each wafer. To make good comparison between the power characteristics of the different wafers, the overlapping parts of the modes having the largest deviation from a straight line through the power curve have been removed. This straight line is obtained using a least squares fit to the measured data. The power is measured with the coupling optics and after that calibrated with a large photodiode. In Fig. 3.12 the optical power ranges are shown for a number of lasers of each wafer. It is between 7 and 9 dBm for the bulk lasers and between 10 and 12 dBm for the quantum well lasers. Clearly the quantum well lasers have a larger output power, in accordance with their lower threshold currents, see section 3.4.

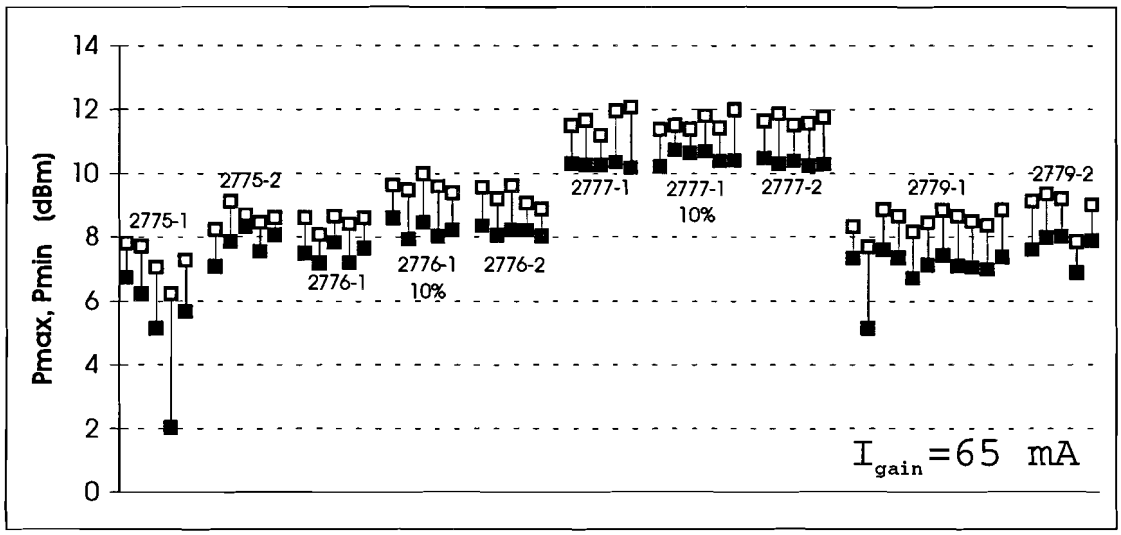

Figure 3.12: **Power ranges for a number of lasers of the 8 wafers. The overlapping parts of the modes have been removed (see text). 10 % indicates devices having a 10 % coating on the front facet (gain section).**

To examine the flatness of the power characteristics, two parameters have been defined, expressing the per mode flatness (a_{average}) and overall flatness (a). The parameter a is the slope of the line through the power characteristic and a_{average} is the average slope of the lines if drawn through the individual modes of the power characteristic, see the inset of Fig. 3.5. If a_{average} is positive the power in a mode decreases if the wavelength decreases, indicating that the PC and DBR sections deliver insufficient gain, see (a) in the inset of Fig. 3.5. If a_{average} is negative the power in a mode increases if the wavelength decreases, indicating that the PC and DBR section deliver too much gain, see (b) in the inset of Fig. 3.5. If a_{average} approaches zero, optimum flatness of the power characteristic is obtained.

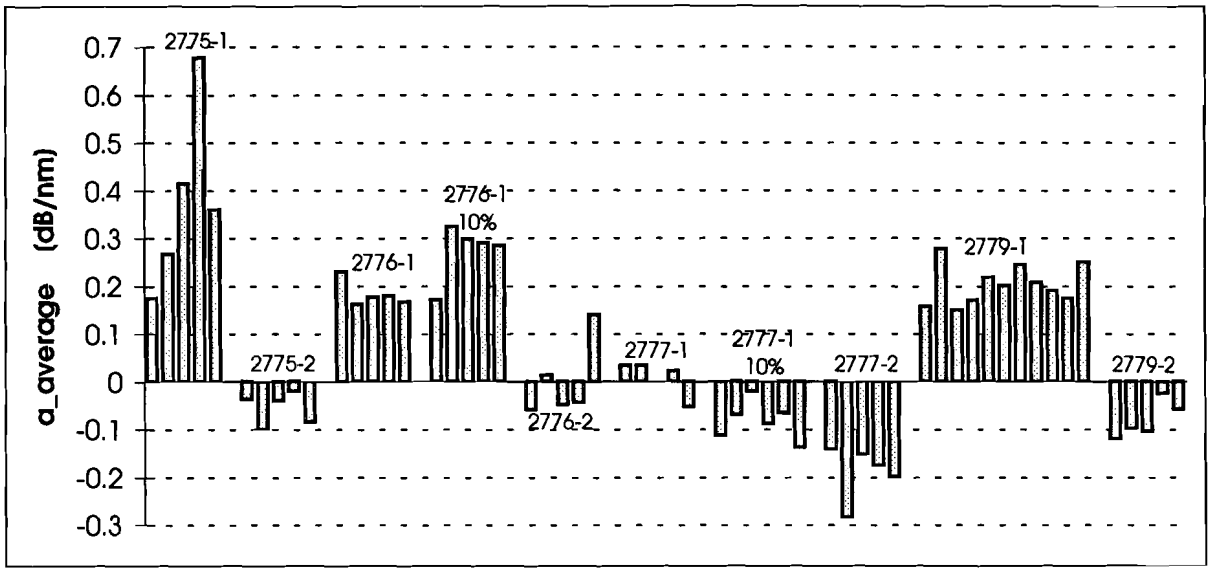

Figure 3.13: The flatness parameter $a_{average}$ for a few lasers of the 8 different wafers. 10 % indicates devices having a 10 % coating on the front facet (gain section).

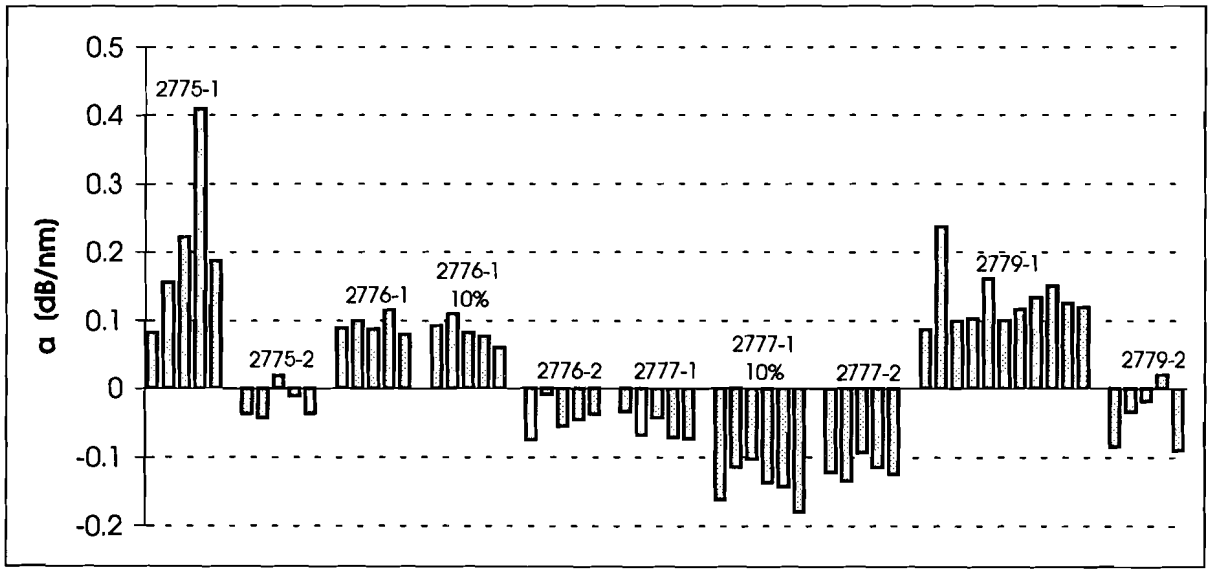

Figure 3.14: The flatness parameter a for a few lasers of the 8 different wafers. 10 % indicates devices having a 10 % coating on the front facet (gain section).

In Fig. 3.13 and 3.14 the parameters a_{average} and a are shown for a number of lasers of each wafer. From these figures, it follows that for the bulk active layer lasers, a $Q_{1.45}$ layer in the tuning sections yields insufficient gain (positive a_{average}) while a $Q_{1.48}$ layers result in too much gain (negative a_{average}). The optimum composition is therefore expected to be found between $Q_{1.45}$ and $Q_{1.48}$, but near $Q_{1.48}$ which yields the lowest $|a_{\text{average}}|$. For the quantum well lasers the optimum is near $Q_{1.45}$.

3.4 L-I characteristic

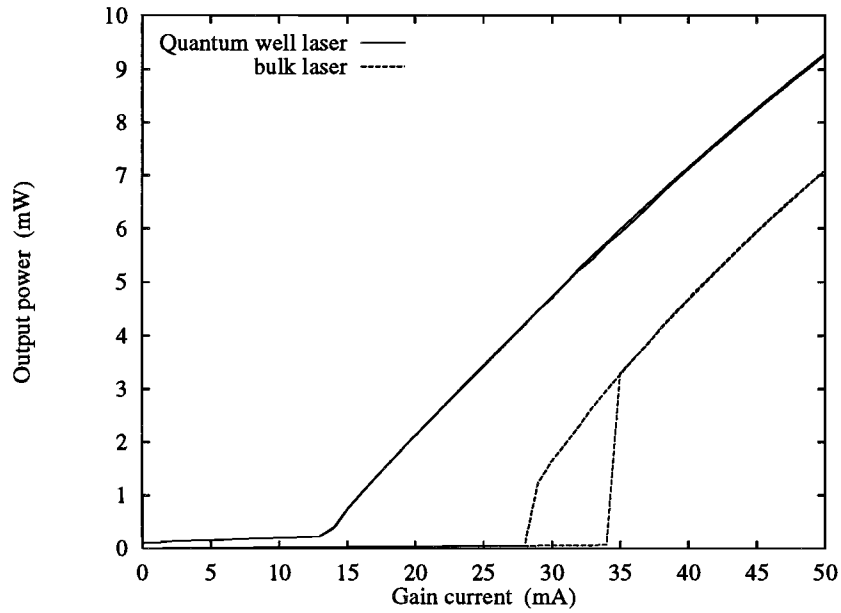

Figure 3.15: L-I curves for a Quantum well and bulk laser at the end of the first mode.

Fig. 3.15 shows the L-I curves for a Quantum well and a bulk laser and Fig. 3.16 shows the threshold currents for one laser of each wafer. The threshold currents are measured for increasing gain current, yielding the on-threshold current $I_{\text{th,on}}$ (upper points), as well as for decreasing current, the off-threshold current $I_{\text{th,off}}$ (lower points). This have been done for four points on the tuning characteristic, namely the beginning and end of the first and last mode. The threshold currents for the bulk active layer and the quantum well lasers are 20-45 mA and 10-20 mA, respectively. The threshold currents exhibits hysteresis, $I_{\text{th,on}} > I_{\text{th,off}}$, for the bulk active layers, except at the end of the tuning characteristic. Furthermore it is observed that sometimes mode jumps in the wavelength occur, if the gain current is varied. By injecting current in the gain section, the refractive index is changed, resulting in a shift of the lasing wavelength, which in turn can cause a mode jump to occur.

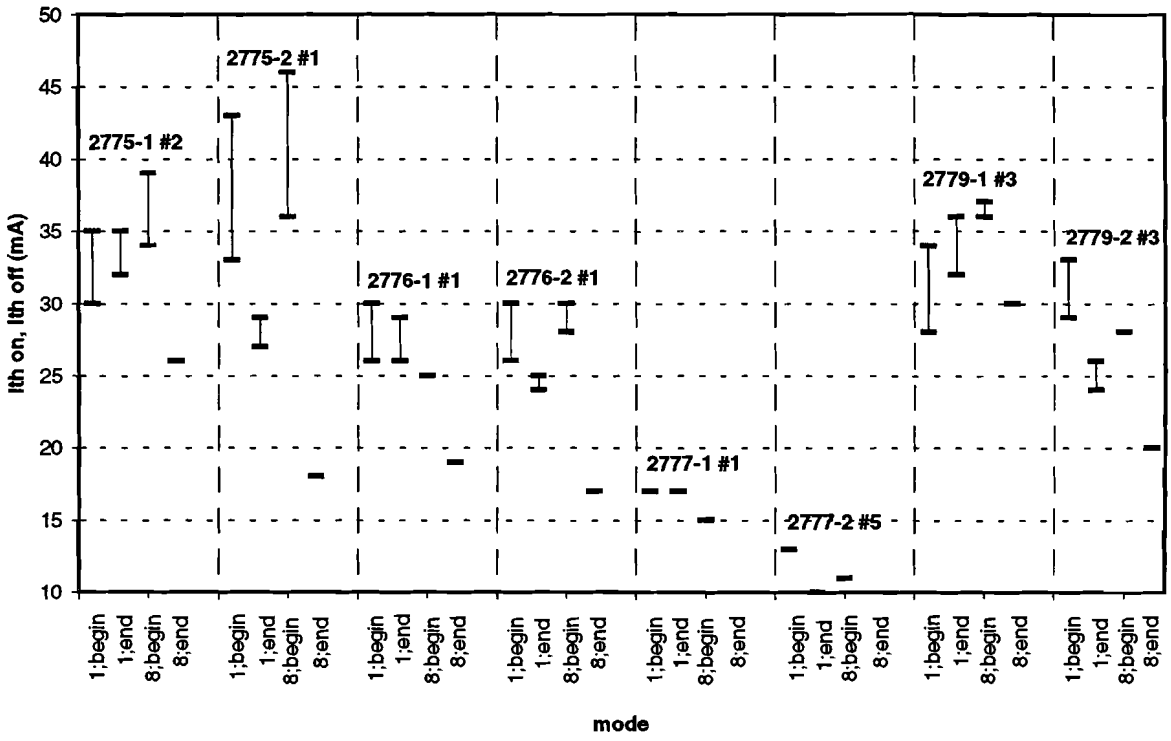

Figure 3.16: $I_{\mathrm{th,on}}$ (upper points) and $I_{\mathrm{th,off}}$ (lowest points) for 8 lasers (8 different wafers). The threshold currents are measured at the beginning and end of the first and last mode.

3.5 Linewidth

To measure the linewidth, the lowest part of the measurement setup in Fig. 3.1 is used. During the measurements of the linewidth, half of the light is coupled by the 3-dB coupler into an Acousto-Optical Modulator (AOM), which shifts the wavelength of the light by 80 MHz. For breaking the coherence of the light, the light is lead through 3.3 kilometre of fibre. Then the light is recombined together with the input signal in the 3dB-coupler. The output of the coupler is detected using a photodiode, and the resulting signal is an electrical spectrum at a center frequency of 80 MHz. The Full Width at Half Maximum (FWHM), i.e. the width of the peak where the power has decreases by 3 dB, which can be measured using an electrical spectrum analyzer, yields twice the linewidth of the laser. In

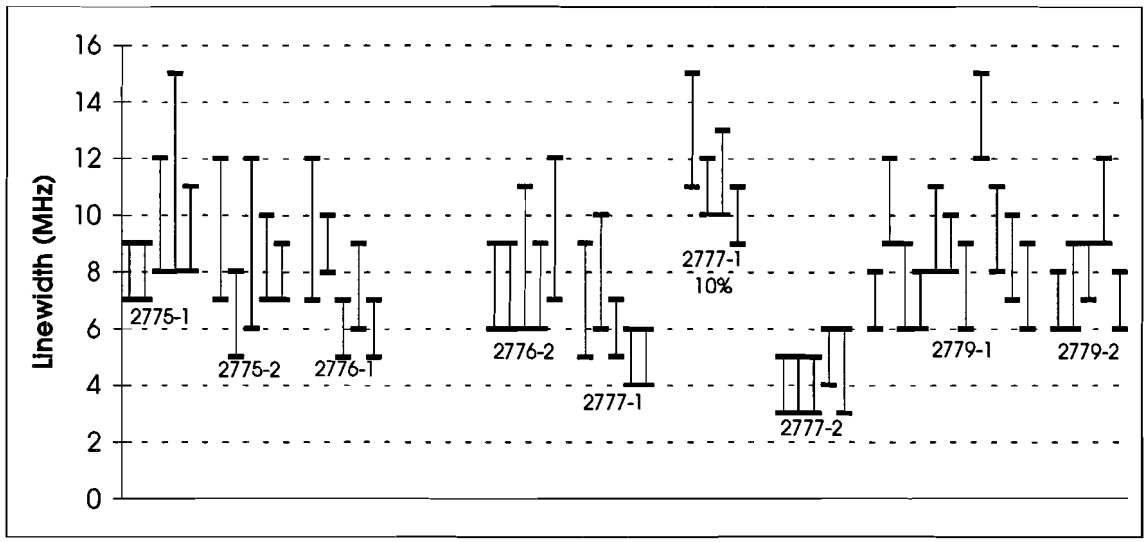

Figure 3.17: **The linewidth ranges for a number of lasers of the 8 different wafers. 10 % indicates devices having a 10 % coating on the front facet (gain section).**

Fig. 3.17 the linewidth ranges are drawn for a number of lasers of the 8 different wafers. From this figure, it follows that the quantum well lasers, MOQT2777-1 and MOQT2777-2, have the smallest linewidth. The linewidth of a laser is primarly determined by the linewidth enhancement factor β_c, which decreases with increasing gain coefficient a_1. With a proper design of the laser, the gain coefficient can be doubled in quantum well lasers as compared to bulk active layer lasers [3]. This leads to a decrease of the linewidth for the quantum well lasers as observed in Fig. 3.17. From the measurements it is found that the linewidth at the end of the tuning characteristic, i.e. for large PC and DBR currents, increases rapidly. The linewidth broadening is determined by the fraction of spontaneous emission, originating in the PC and DBR section, which is coupled into the lasing mode [6]. If the PC and DBR currents increase, the spontaneous emission increases as well, resulting in an increase of the linewidth.

4. Dynamic properties

When a small a.c. signal is applied to one of the sections of the 3-section DBR laser, the output power experiences a small variation in intensity (Amplitude Modulation). Variations in the current lead to variations in the refractive index as well, which in turn result in variations in the wavelength of the laser (Frequency Modulation). AM modulation and FM modulation are thus always present at the same time. AM and FM modulation of the 3-section DBR laser can be applied to any of the three sections, with each section having its own frequency response and residual FM or AM modulation. To measure the AM and FM response of the three sections of the laser, an a.c. signal is applied to one of the sections using the measurement setup of Fig. 3.1. The AM-response can be directly measured using a photodiode, which converts the intensity modulation of the light to an electronic AM modulated signal which can be measured using a spectrum analyser. The FM response can be transformed into an AM modulated signal by means of a Mach-Zehnder Interferometer (MZI). In the MZI the light is splitted by a 3dB coupler into two parts, which are coupled into two short fibers with a length difference of 0.5 cm. This causes a difference in phase of the light at the end of the fibers. Then the light is combined again using a second 3 dB coupler resulting in an interference pattern.

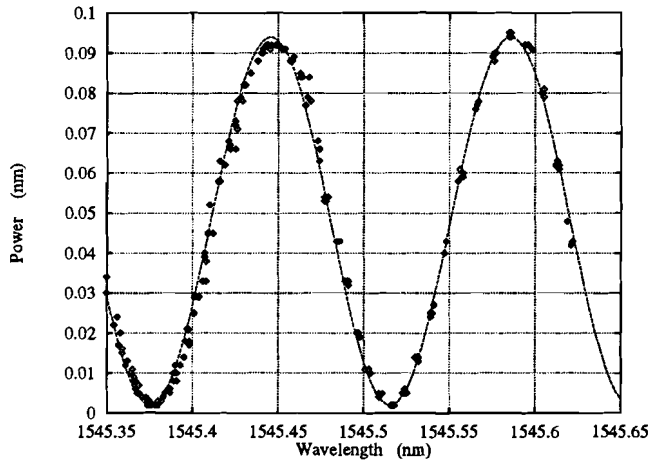

Figure 4.1: The MZI transfer funcion. The dots present the measured values and the solid line is the fitted line between them.

In Fig. 4.1 the transfer function is drawn of a MZI which is given by $A(1+\cos(\phi))$. Here A is a constant and ϕ is the phase difference between the ends of the two fibers and is dependent on the wavelength of the light. The output of the MZI has maxima at a phase difference of $2m\pi$, where m is an integer, and minima at a phase difference $(2m+1)\pi$. To reduce distortions during measurements of the FM-response, it is important to adjust the

wavelength of the laser to the center of the linear part of the MZI transfer function. In addition, the wavelength deviation must not be larger than 0.14 nm (2.5 GHz) to remain inside the lineair region.

4.1 AM-response

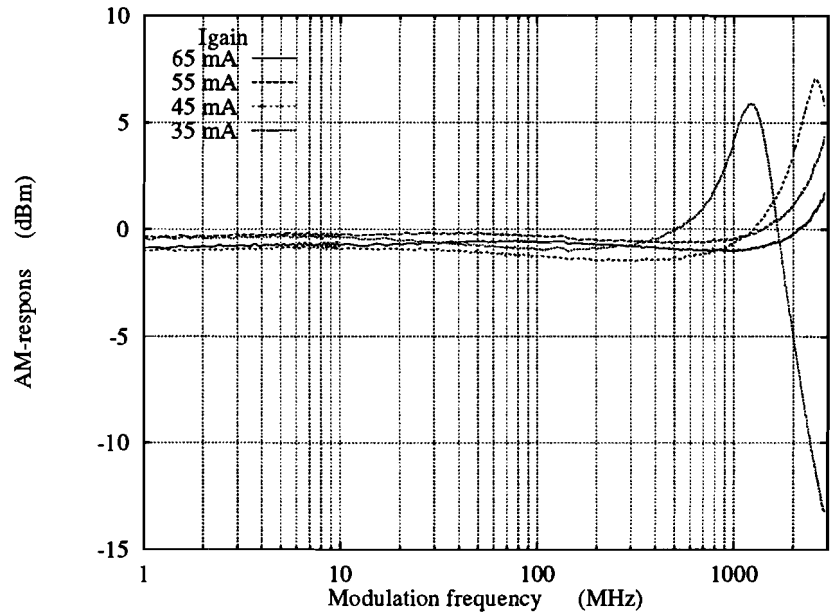

Figure 4.2: The AM-response of the gain section for different gain currents. I_{PC} = 5.8 mA, I_{DBR} = 47 mA.

From Fig. 4.2, which shows the AM respons of the gain section for different gain currents, it is observed that the AM response is nearly constant until the relaxation oscillation frequency is reached, which causes a high peak in the AM response. The relaxation oscillations are caused by an intrinsic resonance, in which energy stored in the system oscillates back and forth between the electron and photon populations, if the gain current increases rapidly from a steady state to a final value. From [3] it follows that the angular frequency of the relaxation oscillations can be written as

$$\Omega_R = G_N \frac{(I_{gain} - I_{th})}{e} \tag{4.1}$$

where G_N is the gain derivative and is a material parameter. The frequency of the relaxation oscillations is about 5 GHz, and is nearequal for the different wafers. From Eq. (4.1) it is observed that if the gain current decreases the relaxation oscillation frequency shifts to shorter frequencies as is also observed in Fig. 4.2.

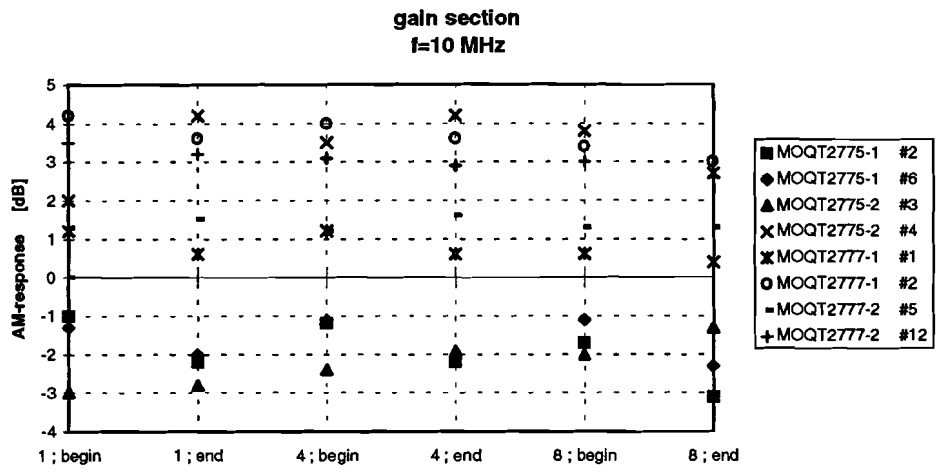

Figure 4.3: **The AM-response of the gain section for 2 lasers of 4 different wafers. The frequency is 10 MHz.**

The AM-response of the gain section is shown in Fig. 4.3 for a number of lasers. The AM response is independent of the wavelength and doesn't vary much among the different wafers. The AM respons of the different wafers is between the -3 and +4 dB and the variations are presumable the result of variations in the incoupling. The AM response is measured on a flat part of the AM responss, and a frequency of 10 MHz is chosen.

4.2 FM-response

A method to measure the FM response is the use of a MZI, which converts the FM-response to an AM response which can be measured with a spectrum analyzer. During the measurements of the FM response there is, in addition to the FM response, always the AM response at the output of the MZI. If the FM response is much larger than the AM response, the latter does not affect the measurement of the FM response. Measurements of the FM response of the gain section could not be made reliably with a MZI due to the residual AM response. The FM response is normally expressed in MHz/mA, and this is not possible with a MZI and therefore calibration is necessary. For the calibration, the FM respons is made visible with a scanning Fabry Perot etalon at one modulation frequency. Then the power of the modulation signal is tuned untill the optical carrier wave disappears, modulation index $m \approx 2.4$, and only the sidebands remain. From this modulation signal power it is possible to calculate the FM-respons by

$$f_\Delta = \frac{f_\mathrm{m}\, m}{I_\mathrm{m}} \tag{4.2}$$

where f_Δ is the FM deviation in Mhz/mA, f_m the modulation frequency and I_m the modulation current. After that, the entire FM response, which is measured with the MZI, can be calibrated.

The FM responses of the DBR and PC sections are much larger than the AM response and therefore a reliable measurement of the FM response is possible using the MZI technique. In Fig. 4.4 an example is given of the FM response of the DBR section, and in Fig. 4.5 the FM responses and bandwidths of the FM response are drawn for a number of lasers. The FM responses are measured on a flat part of the curve (chosen is a frequency of 10 MHz). From Fig. 4.5 if follows that the FM response decreases with decreasing wavelength. The slope of the tuning characteristic is large at small DBR currents (long wavelengths) and small at large DBR currents (short wavelengths), see Fig. 3.2. This means that at the begin of the curve, the wavelength is very sensitive to variations in the DBR current, which implies a large FM response; and at the end of the curve the sensitivity to the DBR current is small, and the FM response is small. On the other hand, the bandwidth increases with decreasing wavelength. This is due to the fact that the maximum speed of modulation increases if the carrier density increases [3]. The differences in FM responses and bandwidths of FM responses of the wafers are small except at the last points of the tuning curve. The DBR current at these points is near the threshold current of the DBR section, resulting in unstable operation of the laser.

In Fig. 4.6 an example is given of the FM response of the PC section, and in Fig. 4.7 the FM responses and bandwidths of the FM response are drawn for a number of lasers. The FM responses are measured on a flat part of the curve (chosen is a frequency of 10 MHz). From Fig. 4.7, it follows that the FM response and the bandwidth are nearly the same at the begin of the modes. This is also true for the end of the modes. The reason is that the PC currents at the begin of the modes and at the end of the modes are equal. The slopes of the $\lambda(I_{PC})$ characteristics are at the begin of the modes larger than at the end of the modes, see Fig. 2.7. The result is a larger FM response at the begin of the modes and a smaller FM response at the end of the modes. The reason for this effect also is due to the fact that the maximum speed of modulation increases if the carrier density increases. The differences in FM responses and bandwidths of FM responses of the wafers are small except at the last points of the tuning curve. The DBR current at these points is near the threshold current of the DBR section, resulting in unstable operation of the laser.

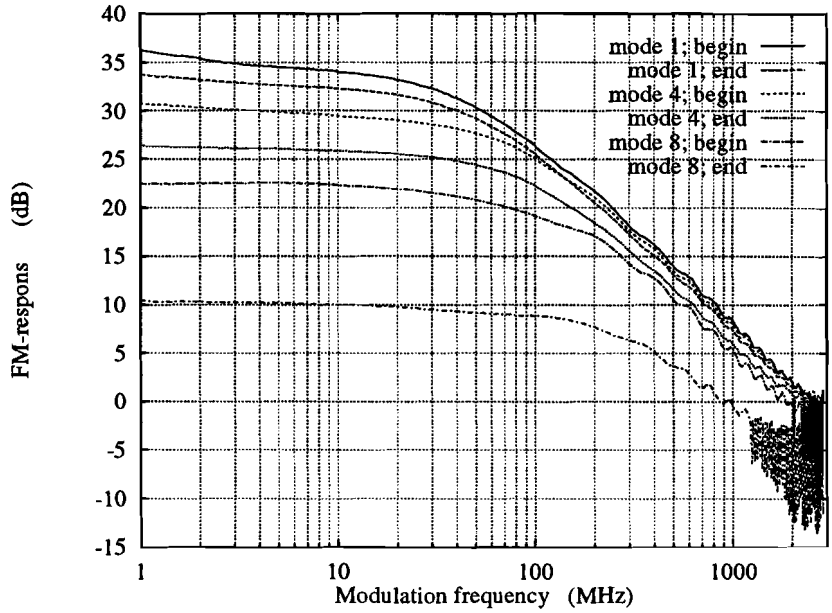

Figure 4.4: The FM-response of the DBR section at 6 different positions on the tuning curve. 0 dB corresponds to 100 MHz/mA.

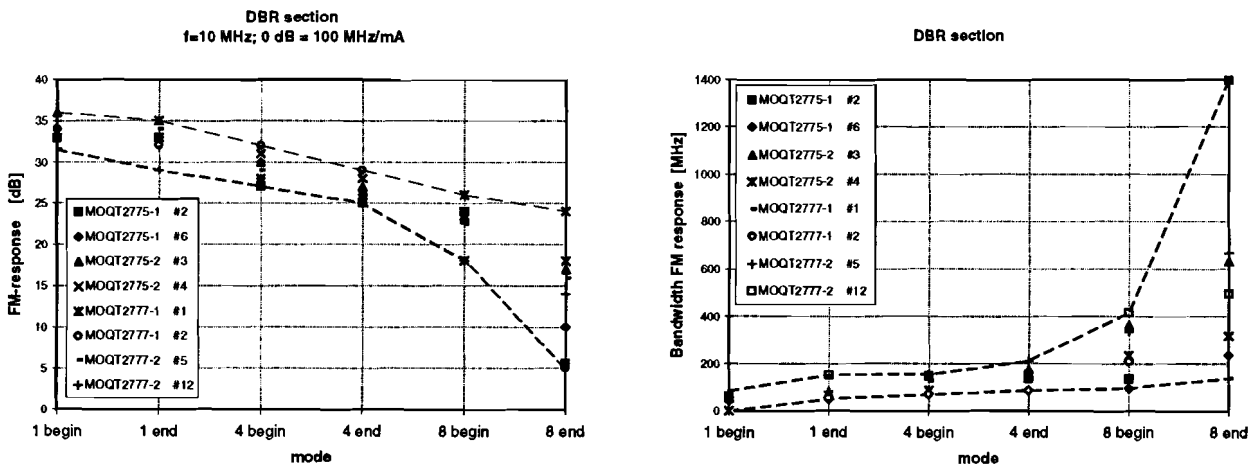

Figure 4.5: The FM-response and bandwidth of the DBR section for 8 lasers (4 different wafers). The FM response is measured at six points on the tuning curve, begin and end of the first, fourth and eighth mode. The modulation frequency for the measurements of the FM response is 10 MHz and 0 dB corresponds to 100 MHz/mA.

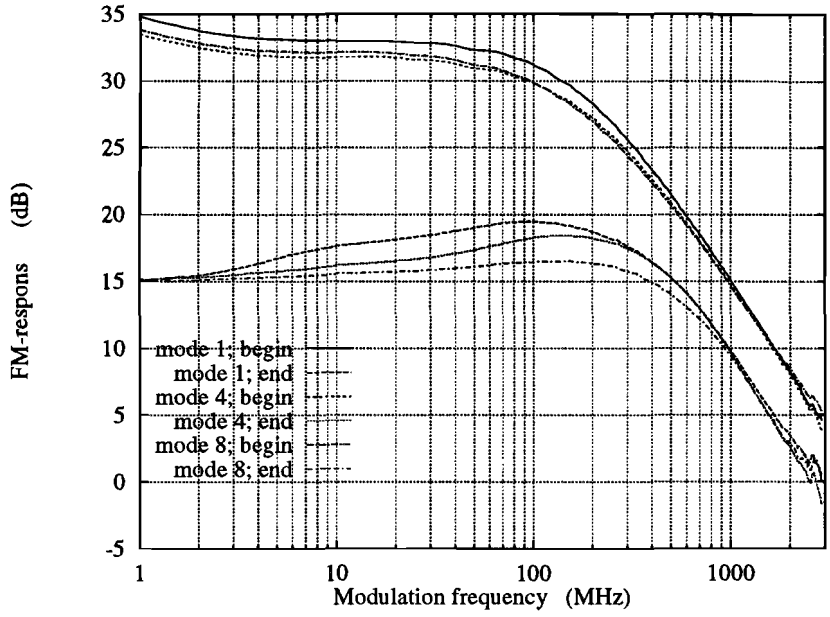

Figure 4.6: The FM-response of the PC section at 6 different positions on the tuning curve. 0 dB corresponds to 100 MHz/mA.

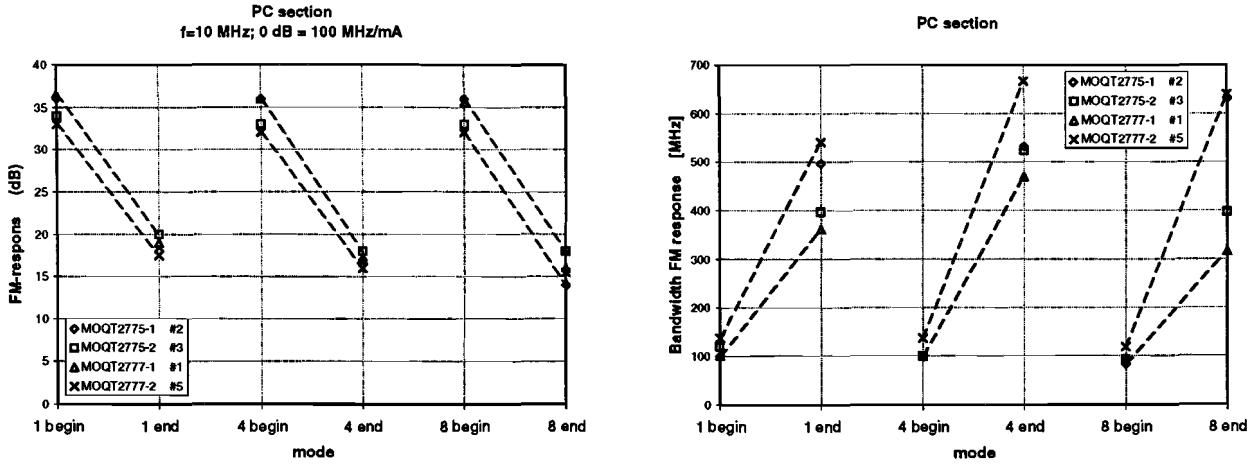

Figure 4.7: The FM-response and bandwidth of the PC section for 4 lasers (4 different wafers). The FM response is measured at six points on the tuning curve, begin and end of the first, fourth and eighth mode. The modulation frequency for the measurements of the FM response is 10 MHz and 0 dB corresponds to 100 MHz/mA.

5. Application of the 3-section DBR laser as a wavelength converter.

5.1 Introduction.

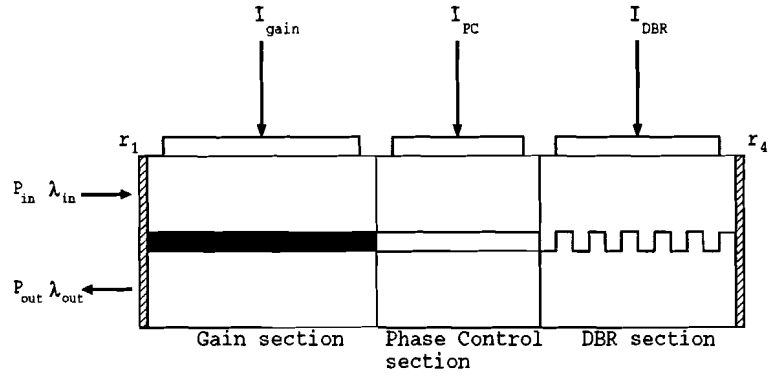

Figure 5.1: Schematic of a DBR wavelength converter.

A schematic diagram of a DBR laser used as a wavelength converter is shown in Fig. 5.1. Wavelength conversion is accomplished as follows: The DBR laser is biased above threshold and oscillating at a wavelength λ_{out}. An intensity modulated optical input signal with wavelength λ_{in} is injected into the gain section of the laser. This input signal causes stimulated recombination resulting in additional depletion of free carriers and consequently a modulation of the gain. The output power reflects this gain modulation, carrying the same (but inverted) information as the input signal. As a result, all-optical wavelength conversion from wavelength λ_{in} to wavelength λ_{out} has been performed. The lasing wavelength λ_{out} can be tuned over the entire wavelength range of the DBR laser by adjusting the PC and DBR currents.

The input power is of considerable importance since the injected optical signal should have an intensity comparable to that of the lasing mode to obtain the required gain saturation. Because the reflectivity of an uncoated facet is approximately 30%, the power actually injected into the gain section is reduced. By applying a 10% reflection coating to the gain section facet, it is possible to couple more signal power into the gain section, see Fig. 5.2. For the cleaved facet ($r_1 = 30\%$) an input power of +5 dBm is necessary to reduce the output power by 3 dB, while application of a 10% reflection coating reduces the required power to only -1 dBm [8]. This is due to a higher carrier concentration which is a

result of a higher gain, see Eq. (2.7), as a result of the increase in mirror loss, see Eq. (2.8). In addition, there is a higher coupled input power into the cavity.

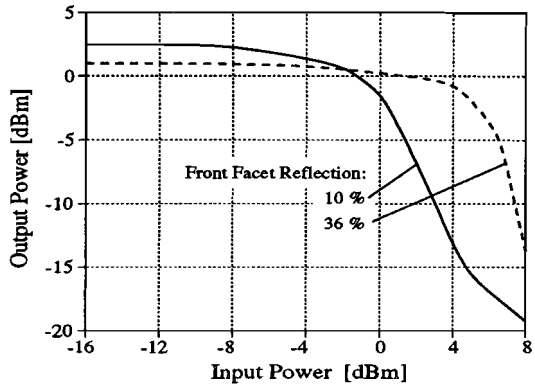

Figure 5.2: **Output power at wavelength λ_{out} versus input power at wavelength λ_{in} with the front facet reflection r_1 as a parameter. (After Ref. [8])**

The input power required for efficient wavelength conversion can also be reduced by decreasing the gain current, see Fig. 5.3. This figure shows the output extinction ratio, which is the ratio of P_{max} and P_{min}, as a function of the gain current with the average input power as parameter [8]. A decreasing output extinction ratio is observed with increasing current and decreasing input power. Furthermore, it is observed that an extinction ratio enhancement can be obtained. Finally, if the gain current is decreased, the rise and fall times increase, resulting in decrease of the bit rate of wavelength conversion that can be obtained [8].

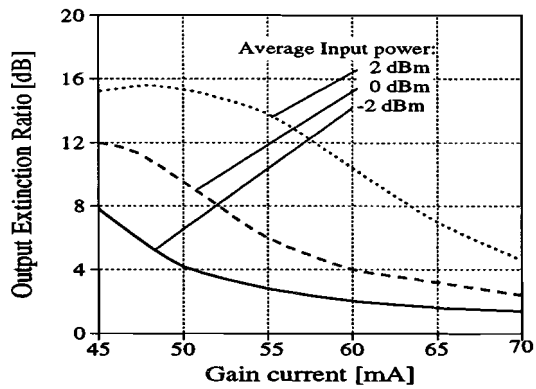

Figure 5.3: **Output extinction ratio as a function of the gain current with the average input power as a parameter. The input extinction ratio is 10 dB. (After Ref. [8])**

5.2 Reduction of the input power

For the measurement of the $P_{out}(P_{in})$ curves with various parameters, the measurement setup of Fig. 5.4 is used. The input signal is provided by a DFB laser at a wavelength of λ_{in} = 1538.4 nm or λ_{in} = 1550.3 nm, and is amplified by an Erbium Doped Fiber Amplifier (EDFA) to a power of about +13 dBm. Next, it is fed through a variable optical attenuator and a polarisation controller. Finally, light is coupled into and out of the DBR laser using a 3 dB-coupler and a tapered fiber. The input signal is partially reflected by the DBR front facet and will contribute to the measured output power. Therefore an optical band pass filter is used to remove this signal.

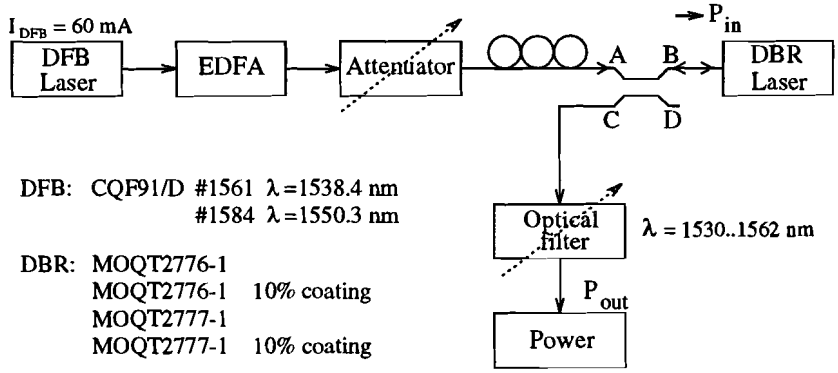

Figure 5.4: **Measurement setup to determine the $P_{out}(P_{in})$ curves. A tapered fiber is used to couple light in and out of the DBR laser.**

In Fig. 5.5 the measured $P_{out}(P_{in})$ curves are drawn for a bulk active layer laser (MOQT2776-1) and a Quantum Well laser (MOQT2777-1) without coatings on the front facet and a bulk active layer laser with a 10%-coating (MOQT2776-1 10%). The curves are measured for 3 gain currents. In Fig. 5.6 the power reductions of the three lasers are shown at four wavelengths. From these figures it is observed that the power reduction (I_{gain} = 65 mA) is about 0.5 dB for the uncoated bulk laser and 2 dB for both the coated bulk and Quantum Well lasers. For low gain current (I_{gain} =45 mA), the power reduction for the coated laser increases rapidly, from 3.5 dB to 14.5 dB, when the wavelength decreases. This is presumable due to the decreasing output power ($\approx$ 1 dB) at the end of the tuning characteristic.

During measurements of the $P_{out}(P_{in})$ curve of the Quantum Well lasers with a 10% coating, wavelength jumps are observed. Due to the 10% coating, a larger fraction of the power resulting from residual reflections in the measurement setup is coupled back into the laser, leading to a substantial increase of the feedack noise and linewidth. Application of an Anti-Reflection coating to the fiber tip is expected to help decreasing the reflected power.

With decreasing gain current, the power reduction increases, but less with increasing

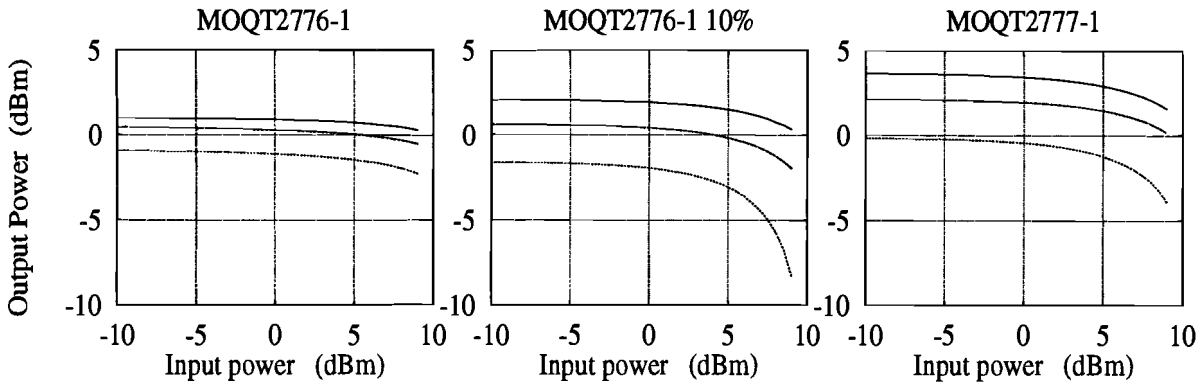

Figure 5.5: Power reduction as function of the input power at 3 gain currents of a MOQT2776-1 and MOQT2777-1 laser without coating and a MOQT2776-1 laser with a 10%-coating. From top to bottom the gain currents are 65, 55, and 45 mA. λ_{in} =1538.4 nm, I_{PC} =28 mA and I_{DBR} =5 mA. The measured output power is attenuated through the optical filter and the 3 dB-coupler by approximately 6 dB.

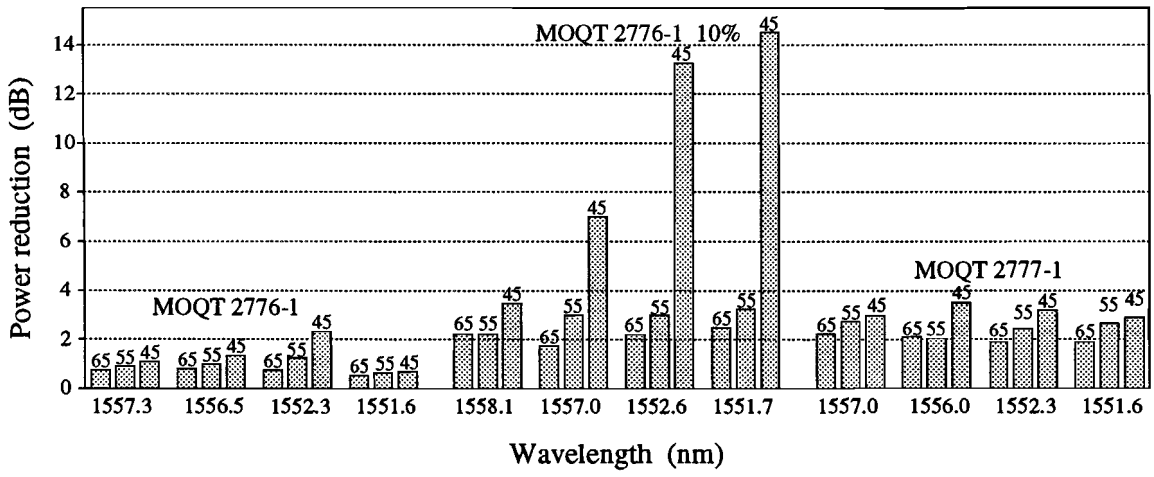

Figure 5.6: Power reduction as function of the wavelength and gain current of 3 lasers. λ_{in} =1538.4 nm and P_{in} =9 dBm. The output wavelengths are at the beginning and end of the first and last mode on the tuning curve.

wavelength within the same mode of the DBR laser, as shown in Fig. 5.6. To obtain the best conversion performance, the gain peak of the gain section should be close to the input wavelength. The gain spectrum can be obtained by measuring the spontaneous emission characteristics of the laser just below threshold, see Fig. 5.7. The peaks at $\lambda \approx 1555$ nm originate from the reflectance of the DBR grating, indicating the Bragg wavelengths at which the laser will operate if biased above threshold. From Fig. 5.7 it follows that the optimum input wavelength for a Quantum Well laser is near 1520 nm, while for the bulk active layer device is close to 1555 nm. The latter nearly coincides with the output wavelength and therefore an input wavelength should be chosen just outside the gain peak.

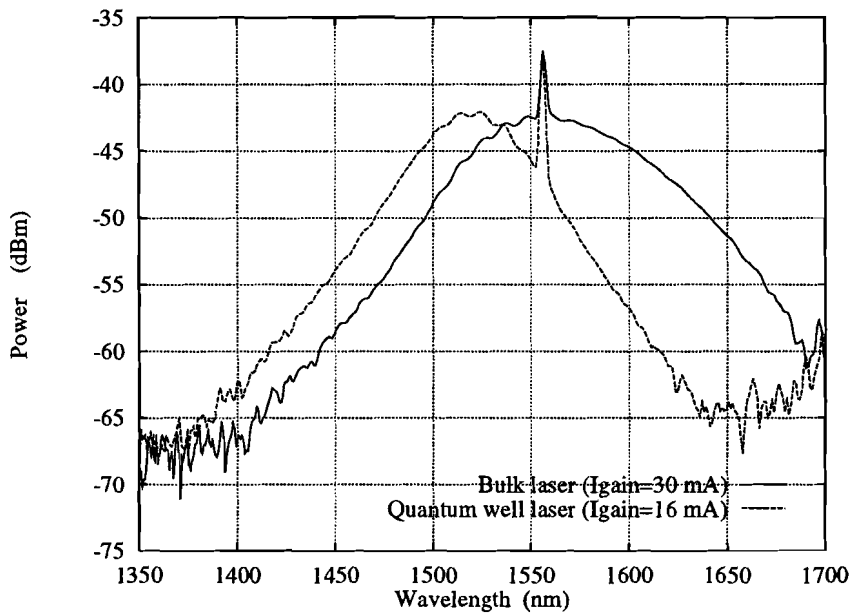

Figure 5.7: **Spontaneous emission characteristics of a bulk active layer and a Quantum Well laser. (I_{PC}=2 mA and I_{DBR}=2 mA).**

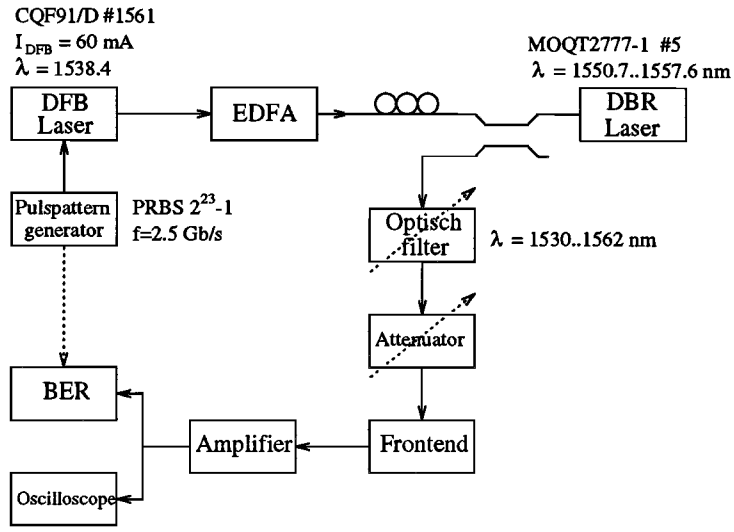

Figure 5.8: Measurement setup.

5.3 System experiments

The measurement setup is shown in Fig. 5.8. The DFB laser (λ_{in} = 1538.4 nm) is modulated by a $2^{23}-1$ PRBS signal at 2.5 Gb/s, a peak-to-peak current of 20 mA and a output exinction ratio of 5.4 dB. The resulting output signal, shown in Fig. 5.9, is injected into the DBR laser with an average power of +8dBm. The Quantum Well lasers with $Q_{1.48}$ tuning layer exhibit the highest output power and a high power reduction and therefore have been used in these experiments. The 3-section DBR laser outputs an inverted version of the signal at a wavelength of λ_{out} = 1556.0 nm, which is shown in Fig. 5.9. The converted signal is measured with a sampling oscilloscope or a Bit Error Rate (BER) meter. Fig 5.10 shows the output extinction ratio as a function of the gain current, which increases with decreasing gain current. If the gain current is below 54 mA, an improvement in the extinction ratio is observed. Fig. 5.11 shows an eye pattern of the converted signal at an input power at the frontend of -10 dBm and Fig. 5.12 shows BER measurements of the DFB signal, EDFA signal, and converted signals at four wavelengths. For direct detection of the DFB signal, the sensitivity of the system is -19 dBm at a BER of 10^{-9} and the penalty for the EDFA is 1 dB. This penalty is due to fluctuations in the output power of the EDFA. The penalty for wavelength conversion is 2 dB at the beginning and 4 dB at the end of the tuning curve. The reason for the larger penalty at the end of a lasing mode on the tuning curve is not understood yet. It may due to an increased feedback senitivity (the fiber chip coupling is established using a tapered fiber, without an optical isolator) at the end of the tuning range, resulting in an increased noise level, however, additional measurements are required to resolve this issue.

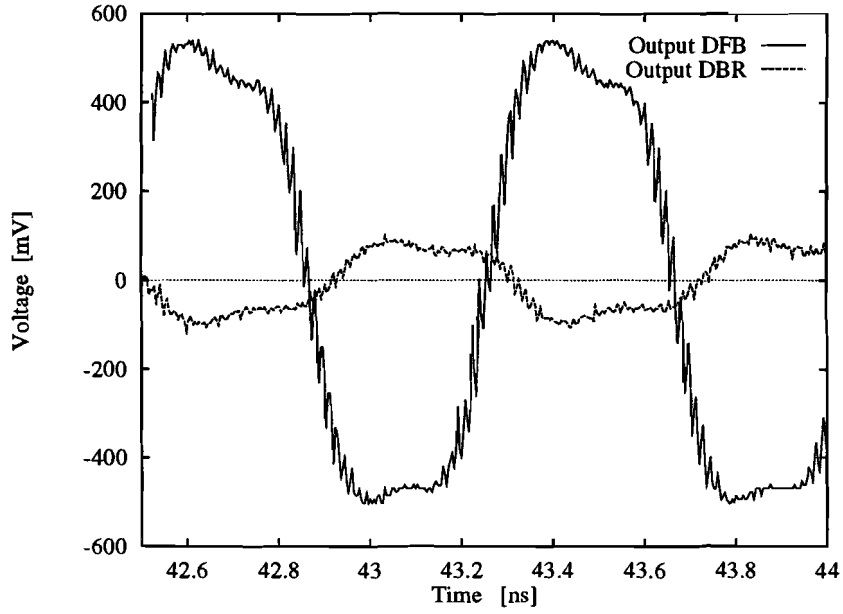

Figure 5.9: Puls pattern output of the DFB laser (without amplifier), as well as the converted signal (with amplifier). I_{DFB} =60 mA, λ_{in} =1538.4 nm, $I_{\mathrm{DBR,gain}}$ =65 mA and λ_{out} =1556.0 nm

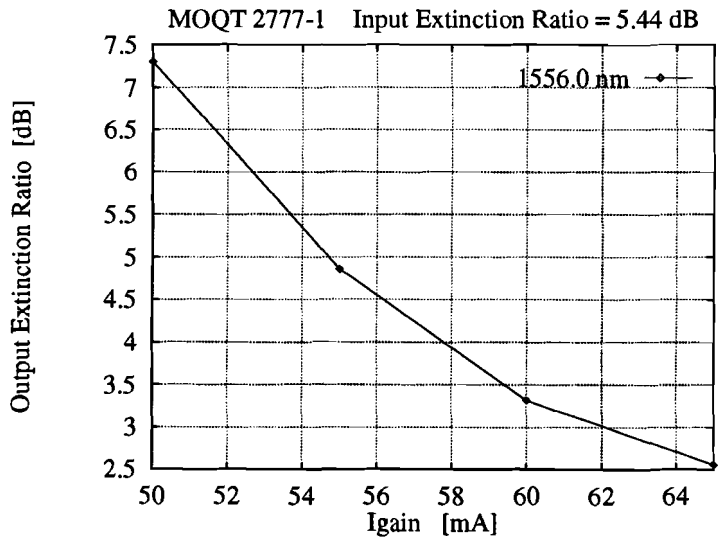

Figure 5.10: Output extinction ratio as a function of the gain current. λ_{in} = 1538.4 nm.

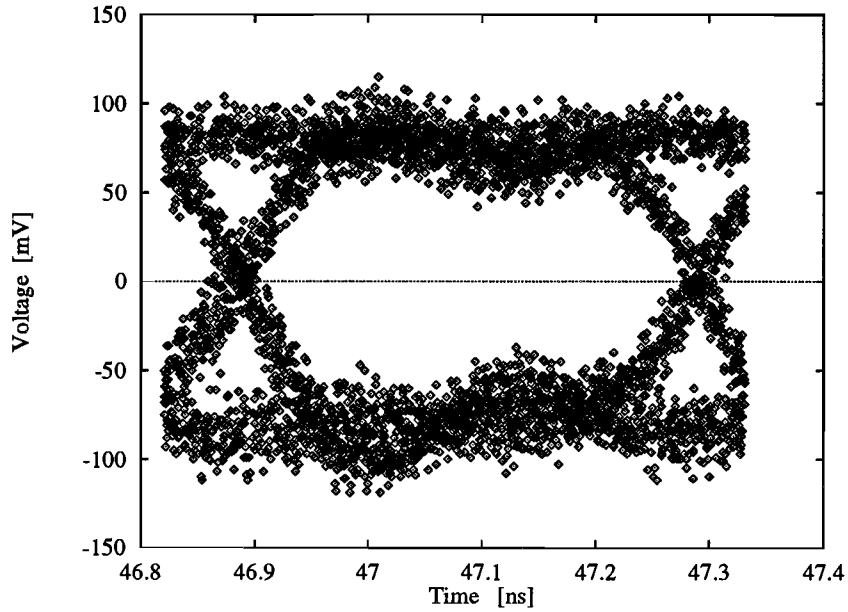

Figure 5.11: **Eye pattern of converted signal, λ_{out} =1556.0 nm, P_{PD} =-10 dBm.**

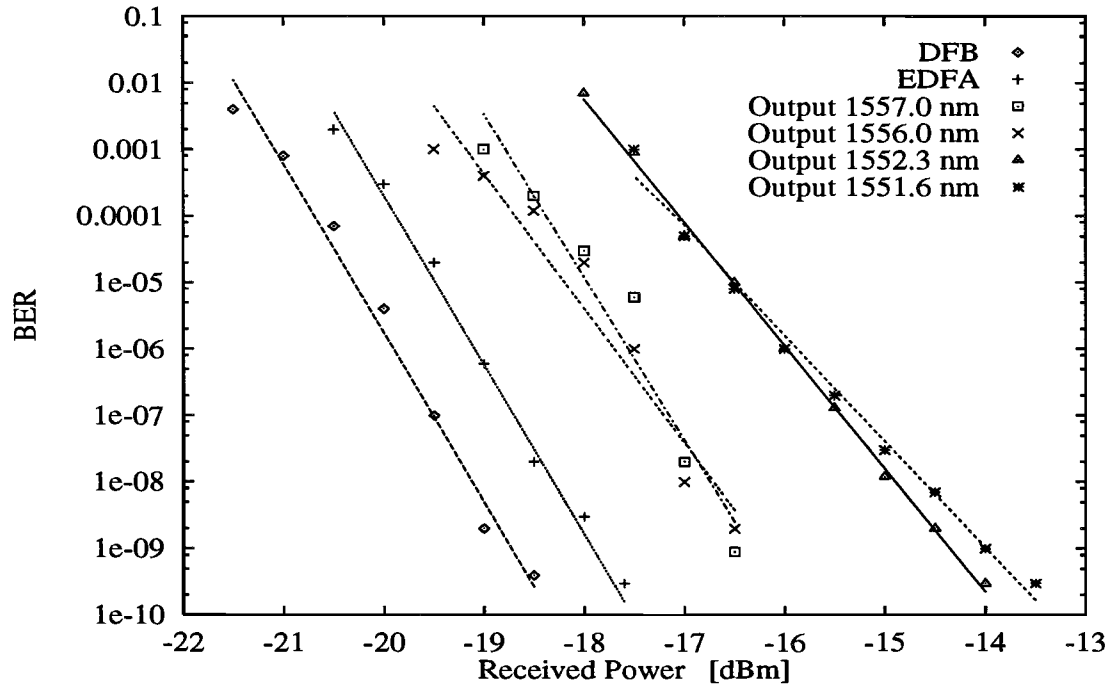

Figure 5.12: **BER measurements. The output wavelengths are at the beginning and end of the first and last mode on the tuning curve.**

6. Conclusions

In this report, a description is given of the operation and characterization of a tunable three section DBR laser and its application as a wavelength converter. Tabel 6.1 shows a summary of the static properties of the lasers:

		min.	max.	unit
Wavelength range		1544	1565	nm
Tuning range*		5	7	nm
Power*	(bulk)	7	9	dBm
	(QW)	10	12	dBm
Linewidth *	(bulk)	6	14	MHz
	(QW)	3	6	MHz
Threshold current	(bulk)	20	45	mA
	(QW)	10	20	mA
Gain current		-	100	mA
PC current		-	30	mA
DBR current		-	70	mA

* at 25 °C and 65 mA gain current

Table 6.1: Static properties of the three section DBR laser.

It is observed that application of Quantum Wells in the active layer, as compared to a bulk active layer, results in a higher output power, a lower threshold current, and a narrower linewidth. The wavelength dependence of the output power of the laser can be reduced by choosing the bandgap of the waveguide layer in the PC and DBR section close to the laser wavelength. Then, the PC and DBR sections deliver some amplification, compensating for the losses due to the increase in free carrier absorption with increasing PC and DBR currents. The optimum composition of this layer is expected to be found between $Q_{1.45}$ and $Q_{1.48}$ (near $Q_{1.48}$ for the bulk lasers, and near $Q_{1.45}$ for the Quantum Well lasers).

The dynamic properties investigated consist of the AM and FM responses. The bandwidth of the AM-response of the gain section is determined by the relaxation oscillations and is for all lasers the same. Tabel 6.2 shows the FM responses and bandwidths of the PC and DBR sections, which are the same for all devices.

Wavelength conversion using a 3-section DBR laser has been demonstrated. The required input power for wavelength conversion can be reduced by 1.5 dB by applying a 10% coating to the gain section facet, and by decreasing the gain current. An extinction Ratio enhancement of 2 dB can be obtained by reducing the gain current. The BER penalty for wavelength conversion is 2 dB at the beginning and 4 dB at the end of the tuning range. However, additional measurements are required to investigated this more in detail.

	FM response (Ghz/mA)	Bandwidth (MHz)
DBR section		
begin of tuning range	5.6	100
end of tuning range	0.6	600
PC section		
begin of mode	5.6	100
end of mode	1	500

Table 6.2: Dynamic properties of the three section DBR laser.

Bibliography

[1] Xing Pan et al.,
A THEORETICAL MODEL OF MULTIELECTRODE DBR LASERS,
IEEE Journal of Quantum Electronics, December 1988, Vol. 24, pp. 2423-2432.

[2] A.A.M. Staring et al.,
WAVELENGTH-INDEPENDENT OUTPUT POWER FROM AN INJECTION-TUNABLE DBR LASER,
IEEE Photonics Technology Letters, February 1994, Vol. 6, pp. 147-149.

[3] G.P. Agrawal and N.K. Dutta,
LONG-WAVELENGTH SEMICONDUCTOR LASERS
Van Nostrand Reinhold, 1986, New York.

[4] B. Tromborg et al.,
TRANSMISSION LINE DESCRIPTION OF OPTICAL FEEDBACK AND INJECTION LOCKING FOR FABRY-PEROT AND DFB LASERS,
IEEE Journal of Quantum Electronics, November 1987, Vol. 23, pp. 1875-1889.

[5] W. Streifer et al.,
EFFECT OF EXTERNAL REFLECTORS ON LONGITUDINAL MODES OF DISTRIBUTED FEEDBACK LASERS,
IEEE Journal of Quantum Electronics, April 1975, Vol. 11, pp. 154-161.

[6] G.H. Duan and P. Gallion,
DRIVE CURRENT NOISE INDUCED LINEWIDTH IN TUNABLE MULTIELECTRODE LASERS,
IEEE Photonics Technology Letters, February 1991, Vol. 3, pp. 302-304.

[7] B. Tromborg et al.,
THEORY OF LINEWIDTH FOR MULTIELECTRODE LASER DIODES WITH SPATIALLY DISTRIBUTED NOISE SOURCES,
IEEE Journal of Quantum Electronics, February 1991, Vol. 27, pp. 178-192.

[8] C. Bragaard et al.,
MODELING THE DBR LASER USED AS WAVELENGTH CONVERSION DEVICE,
IEEE Journal of Lightwave Technology, June 1994, Vol. 12, pp. 943-951.